© 2020. Published by The Company of Biologists Ltd | Development (2020) 147, dev180018. doi:10.1242/dev.180018

STEM CELLS AND REGENERATION

RESEARCH ARTICLE

Regulation of embryonic and adult neurogenesis by Ars2

Yang Yu[1,*,‡], Celia Andreu-Agullo[1], Bing Fang Liu[2], Luendreo Barboza[2], Miklos Toth[2] and Eric C. Lai[1,‡]

ABSTRACT

Neural development is controlled at multiple levels to orchestrate appropriate choices of cell fate and differentiation. Although more attention has been paid to the roles of neural-restricted factors, broadly expressed factors can have compelling impacts on tissue-specific development. Here, we describe *in vivo* conditional knockout analyses of murine Ars2, which has mostly been studied as a general RNA-processing factor in yeast and cultured cells. Ars2 protein expression is regulated during neural lineage progression, and is required for embryonic neural stem cell (NSC) proliferation. In addition, *Ars2* null NSCs can still transition into post-mitotic neurons, but fail to undergo terminal differentiation. Similarly, adult-specific deletion of *Ars2* compromises hippocampal neurogenesis and results in specific behavioral defects. To broaden evidence for Ars2 as a chromatin regulator in neural development, we generated Ars2 ChIP-seq data. Notably, Ars2 preferentially occupies DNA enhancers in NSCs, where it colocalizes broadly with NSC regulator SOX2. Ars2 association with chromatin is markedly reduced following NSC differentiation. Altogether, Ars2 is an essential neural regulator that interacts dynamically with DNA and controls neural lineage development.

KEY WORDS: Ars2, SRRT, SOX2, Neurogenesis, Mouse, Transcription, ChIP-seq

INTRODUCTION

Proper regulation of neural stem cell (NSC) lineage progression is essential for embryonic brain development and adult brain function. The mouse forebrain contains three major NSC populations: embryonic NSCs in the ventricular zone (VZ) of the neural tube, adult NSCs in the subventricular zone (SVZ) of the lateral ventricles (LV) and hippocampal NSCs resident in the subgranular zone (SGZ) of the dentate gyrus (DG). All three NSC types undergo similar developmental stages before terminal maturation. NSCs first give rise to intermediate progenitor cells (IPCs), which then become post-mitotic immature neurons. Given appropriate environmental and intracellular cues, these cells will further differentiate into mature neurons with functional connectivity (Kriegstein and Alvarez-Buylla, 2009). Over the past decades, elucidation of transcriptional networks orchestrating proliferation, specification and differentiation has laid the foundation for discovering the molecular mechanisms controlling neural development. Central to these are families of sequence-specific transcription factors, including HMG box factors (such as SOX2) (Ferri et al., 2004; Pevny and Placzek, 2005), bHLH factors (i.e. HES and NeuroD families) (Dennis et al., 2018) and T-box factors (TBR1/2) (Englund et al., 2005).

In addition to sequence-specific transcription factors, transcriptional co-regulators and general chromatin factors are crucial for neural development. For example, the SWI/SNF chromatin remodeling complex mediates NSC proliferation, specification and neural maturation (Lessard et al., 2007). Moreover, multiple members of CHD family chromatin remodelers are mutated in human neural diseases (Li and Mills, 2014) and CHD7, a gene associated with CHARGE syndrome, binds SOX2 and co-regulates genes in NSCs (Engelen et al., 2011). We have also reported RNA-binding protein Ars2 (also known as SRRT) as an unexpected transcriptional regulator of *Sox2* that maintains adult SVZ NSCs (Andreu-Agullo et al., 2012).

Ars2 was originally identified as a developmental locus in *Arabidopsis* (Clarke et al., 1999; Grigg et al., 2005). It is conserved across plants, fungi and metazoans (Prigge and Wagner, 2001), and usually encoded by a single gene in animals. SRRT refers to the plant ortholog SERRATE; however, because of the similarly named Notch ligand Serrate, we prefer the designation Ars2, used hereafter. Ars2 participates in multiple nuclear regulatory complexes, with its best characterized roles relating to the cap binding complex (CBC). The core CBC associates with distinct partners to mediate diverse RNA-processing reactions, and Ars2 functions in multiple CBC subcomplexes. Ars2 promotes 3′ end formation of non-adenylated histone mRNAs via CBC, SLBP and NELF-E (Gruber et al., 2012; Hallais et al., 2013). Ars2 also associates with CBC-PHAX in the CBCAP complex to promote transcriptional termination and 3′ end formation, especially within cap-proximal regions (Andersen et al., 2013; Hallais et al., 2013; Sabath et al., 2013). Finally, Ars2 associates with the CBC-ZC3H18-NEXT (CBCN) complex to facilitate substrate degradation via the RNA exosome (Andersen et al., 2013; Lubas et al., 2011). Notably, CBC subcomplexes such as CBCAP and CBCN have mutually exclusive components (e.g. PHAX versus ZC3H18) and therefore determine distinct RNA fates, although Ars2 appears to be shared by different CBC subcomplexes (Giacometti et al., 2017). By promoting termination and turnover of promoter upstream transcript (PROMPT) enhancer RNA and cryptic non-coding transcripts, Ars2 was proposed as a general suppressor of pervasive transcription (Iasillo et al., 2017).

Beyond the CBC, Ars2 participates in small RNA pathways. Plant SERRATE was originally implicated in nuclear miRNA biogenesis (Lobbes et al., 2006; Yang et al., 2006) by partnering with HYL1, a double stranded RNA-binding protein cofactor for the miRNA-generating RNase III enzyme DCL1. SERRATE promotes accurate (Dong et al., 2008) and efficient (Iwata et al., 2013) cleavage by DCL1. Metazoan Ars2 also links to miRNA and siRNA pathways by associating with RNase III factors (Gruber et al., 2009; Sabin et al., 2009), and is additionally required in transposon silencing by piRNAs (Czech et al., 2013).

[1]Department of Developmental Biology, Memorial Sloan-Kettering Cancer Center, 1275 York Ave, Box 252, New York, NY 10065, USA. [2]Department of Pharmacology, Weill Cornell Medical College, 1300 York Ave, New York, NY 10065, USA.
*Present address: State Key Laboratory of Medical Molecular Biology, Institute of Basic Medical Sciences, Chinese Academy of Medical Sciences and Peking Union Medical College, Beijing 100005, China.

‡Authors for correspondence (yuy@ibms.pumc.edu.cn; laie@mskcc.org)

Y.Y., 0000-0003-3483-3185; E.C.L., 0000-0002-8432-5851

Received 1 May 2019; Accepted 20 November 2019

Development (2020) 147, dev180018. doi:10.1242/dev.180018

Recent studies of *Arabidopsis* miRNA biogenesis provided an unexpected connection of SERRATE to chromatin machinery, via direct interaction with CHR2 (Wang et al., 2018). CHR2 is an ATPase in the SWI2/SNF2 nucleosome remodeling complex, and affects miRNA expression not only through transcription, but also via an inhibitory role in remodeling primary(pri)-miRNAs to prevent their processing (Wang et al., 2018). The mechanistic crossover of post-transcriptional and transcriptional machineries is further emphasized by *Arabidopsis* SERRATE regulating deposition of H3K27me1 by histone methyltransferases ATXR5/6 to control transposons (Ma et al., 2018) and that chromatin-bound SERRATE preferentially acts as a positive transcriptional regulator of intronless genes (Speth et al., 2018).

Here, we extend studies on the role of mammalian Ars2 in neurogenesis (Andreu-Agullo et al., 2012) to embryonic and adult SGZ stages, revealing common and stage-specific effects. Although Ars2 is most well known as an RNA-processing factor, we use ChIP-seq data to broaden its chromatin-based role. Ars2 preferentially occupies active enhancers genome-wide in NSCs but loses these interactions in differentiating neurons. We also revealed that adult-specific deletion of *Ars2* in NSCs causes specific defects in a high-stress behavioral paradigm. This work broadens the regulatory scope of Ars2 in the neuronal lineage.

RESULTS

Ars2 is required for embryonic neocortex NSC proliferation

Ars2 is a conserved eukaryotic gene with essential roles in multiple basic aspects of RNA biogenesis, which might imply ubiquitous regulatory activities. However, we have previously observed that Ars2 protein accumulates dynamically in the adult mouse SVZ: it is high in quiescent NSCs, but much lower in neuroblasts (Andreu-Agullo et al., 2012). We therefore examined Ars2 expression during embryonic NSC specification and differentiation. Immunostaining of E15.5 lateral ganglionic eminence (LGE) showed that Ars2 does not accumulate uniformly with DAPI$^+$ nuclei (Fig. 1A). Instead, Ars2 was higher in ventral VZ SOX2$^+$ nuclei (marking multipotent NSCs), lower in SVZ (containing IPCs and early-born neurons) and elevated in striatum (containing differentiating neurons) (Fig. 1A). Ars2 expression overlapped with mitotic marker phospho-Histone H3 (pH3), but most Ars2$^+$ VZ cells were pH3$^-$ (Fig. S1A). Thus, Ars2 is enriched not only in G2-phase NSCs, but expressed by most VZ cells. Embryonic neocortex single cell RNA-seq data (Loo et al., 2019) corroborated these dynamics: *Ars2* transcripts decreased following NSC specification and differentiation, similar to neural progenitor markers *Nes*, *Sox2* and *Ascl1*, whereas neuroblast marker *Dcx* and postmitotic neuronal marker *Neurod6* accumulated along this cell trajectory (Fig. S1B,C).

We investigated whether this expression pattern might reflect specific genetic roles for Ars2 in neural lineages. Using *hGFAP-Cre* (Zhuo et al., 2001) to delete *Ars2* in NSCs (Fig. 1B), we have previously found Ars2 crucial to maintain adult SVZ NSCs (Andreu-Agullo et al., 2012). To determine whether Ars2 is required in embryonic NSCs, we cultured primary NSCs from E14.5 forebrain. After two passages, neurospheres from *hGFAP-Cre; Ars2$^{fl/fl}$* mutants were smaller than *hGFAP-Cre; Ars2$^{fl/+}$* controls (Fig. 1C), suggesting that Ars2 is required for embryonic NSC expansion as in the adult SVZ.

Deletion of *Ars2* in NSCs causes hydrocephalus and disrupts cerebellum development with variable severity

hGFAP-Cre; Ars2$^{fl/fl}$ mutants were born at Mendelian ratio but exhibited severe brain defects, including reduction of total brain size, absence of hippocampus and enlarged lateral ventricles (Fig. 2A-D). Such defects were potentially consistent with defective NSC expansion. However, these phenotypes were accompanied by damage to the corpus callosum, and variable cortical thinning,

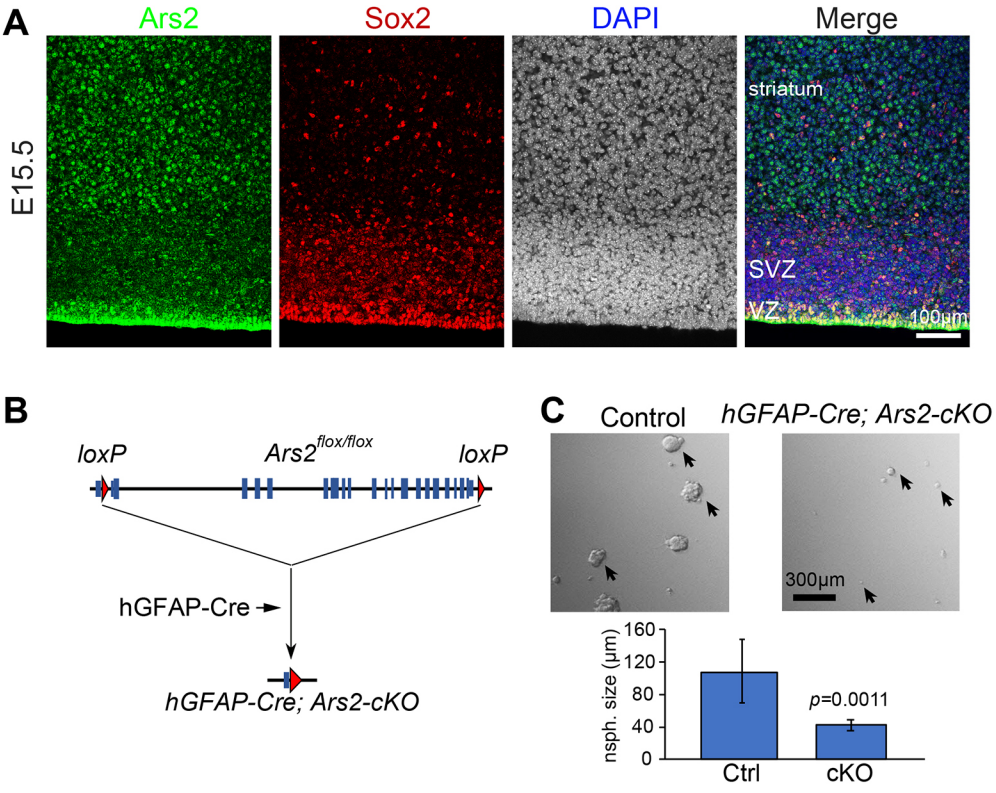

Fig. 1. Ars2 is required for embryonic NSC development. (A) E15.5 ventral forebrain stained for Ars2 (green) shows it is expressed in the ventricular zone (VZ) enriched for SOX2 (red) and in postmitotic neurons in the striatum, but is downregulated in the subventricular zone (SVZ) region. DAPI (blue/grayscale) stains all nuclei. (B) Strategy to generate *Ars2* conditional knockout mice using *hGFAP-Cre*. (C) Neurospheres (nsph.) from *hGFAP-Cre; Ars2$^{fl/fl}$* embryonic forebrain are significantly smaller. Arrows indicate representative neurospheres. *n*=9, two tailed *t*-test; data are mean±s.d.

Development (2020) 147, dev180018. doi:10.1242/dev.180018

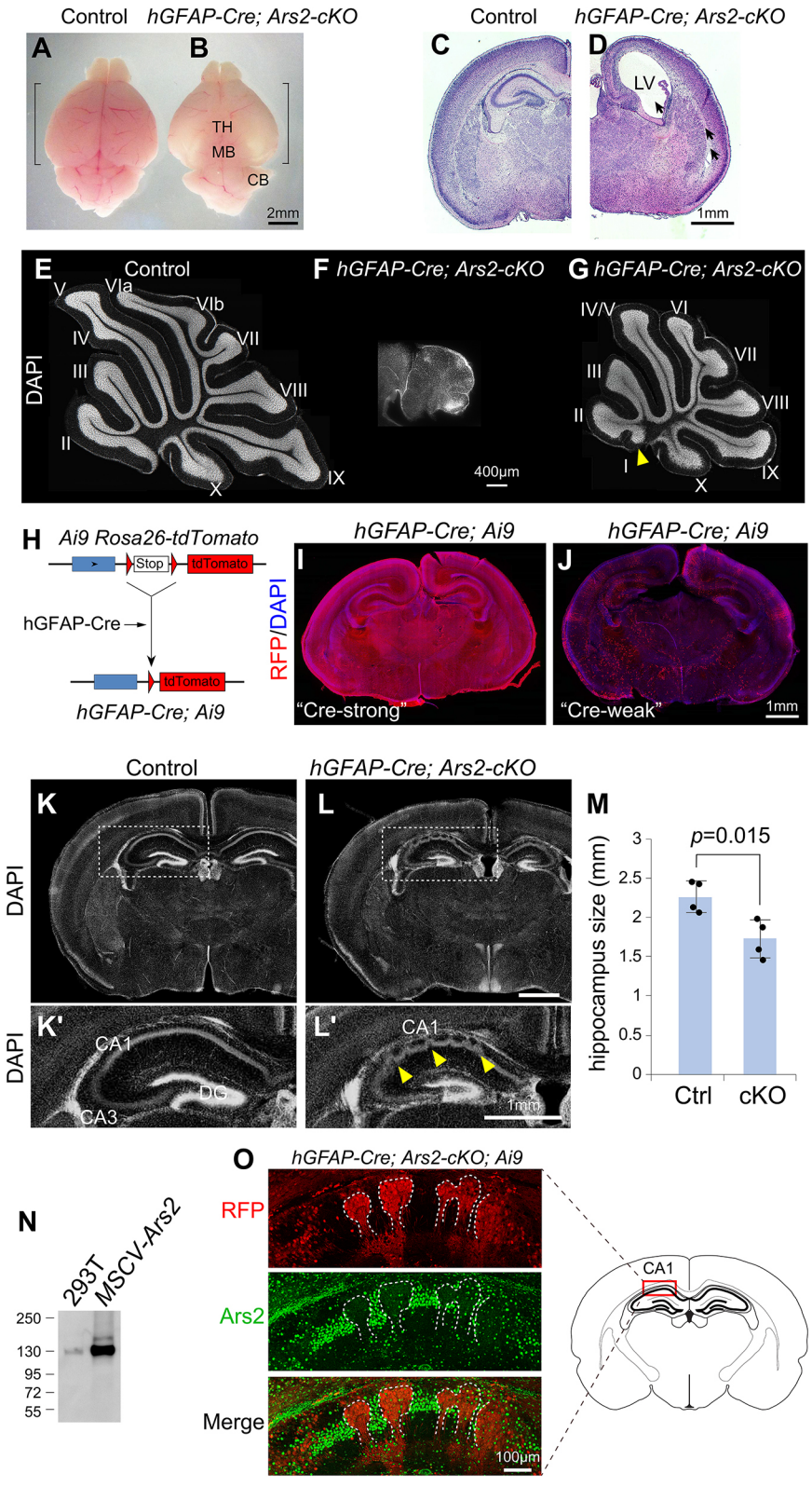

Fig. 2. Mosaic knockout of Ars2 during early neural development. (A,B) Dorsal view of wild-type (control) and *hGFAP-Cre; Ars2*$^{fl/fl}$ brains. The mutant shows reduced cortex (bracketed region), exposing the thalamus (TH) and midbrain (MB), normally not visible in the control *hGFAP-Cre; Ars2*$^{fl/+}$ brain. The cerebellum (CB) spheres are also reduced. (C,D) Hematoxylin and Eosin staining of coronal sections of P5 *hGFAP-Cre; Ars2*$^{fl/+}$ (Control) and *Ars2*$^{fl/fl}$ brains. Arrows indicate enlarged lateral ventricle (LV) and damaged white matter tract. (E-G) DAPI staining on sagittal sections of P15 cerebellar vermis from *Ars2*$^{fl/fl}$ mouse shows abnormal cerebellum foliation with varied severity (F,G) compared with control (E). The arrowhead highlights the appearance of the precentral fissure and lobule I. *n*>20 (strong phenotype) and *n*>15 (weak phenotype) animals were analyzed. Note that initial crosses yielded ~4:1 strong:weak phenotypes, but the weak Cre-dependent effect was segregatable to yield mostly the weak *cKO* phenotypic class for several generations. (H) Strategy to generate *hGFAP-Cre; Ai9[ROSA-flox-stop-flox-tdTomato]* reporter mice. (I,J) Coronal sections of P0 *hGFAP-Cre; Ai9* mice show variable Cre activity. (K-M) DAPI staining on coronal brain sections of P12 mouse with *Ars2* knockout using 'weak' *hGFAP-Cre* line (L,L′) compared with control (K,K′). K′ and L′ show magnifications of the boxed areas in K and L, respectively. Arrowheads indicate the irregular hippocampal CA area. The size of the hippocampus is defined as the least upper bound. *n*=4, two-tailed *t*-test; data are mean±s.d. (N) Western blot validation of new Ars2 antibodies following Ars2 overexpression in 293 T cells. (O) P9 *hGFAP-Cre; Ars2*$^{fl/f}$*; Ai9* hippocampal CA1 region stained for tdTomato (red) and Ars2 (green). Dotted lines highlight the areas with Cre-induced tdTomato that consistently lack Ars2.

which also indicated hydrocephalus (Fig. 2C,D). The possibility of hydrocephaly made it difficult to distinguish cell-autonomous functions of Ars2 from secondary brain damage caused by high brain pressure.

However, we noticed that the fourth ventricle of *hGFAP-Cre; Ars2*$^{fl/fl}$ mice was normal, indicating no hydrocephalus injury to its boundaries, including the cerebellum. *hGFAP-Cre* is expressed by granule cell precursors (GCPs) in the cerebellum external granule layer (EGL) and Bergmann glia. Cerebellum foliation starts from late embryogenesis and continues during the first two weeks after birth (Fig. 2E) (Casper and McCarthy, 2006; Zhuo et al., 2001). Curiously, although all *hGFAP-Cre; Ars2*$^{fl/fl}$ animals exhibited

Development (2020) 147, dev180018. doi:10.1242/dev.180018

phenotypes, we observed dramatic variation in gross cerebellar morphology across individuals. Most *Ars2-cKO* mice (~80%) exhibited severely reduced cerebellar size and arrested cerebellum development. Mature neurons and cerebellar fissures were barely detectable or fully absent (Fig. 2F; Fig. S2A). However, the remaining knockouts (~20%) showed a well-folded cerebellum that was reduced in size (Fig. 2G). Strikingly, these mutants displayed emergence of the precentral fissure (Fig. S2B, arrow) and cerebellum lobule I (Fig. S2B, arrowhead; Fig. 2G, arrowhead), which were absent in control littermates and *C57BL/6* wild type (Sillitoe and Joyner, 2007) (Fig. 2E). *hGFAP-Cre* is not activated in Purkinje cells (Zhuo et al., 2001). Most Purkinje neurons differentiated successfully and migrated into the Purkinje cell layer, with small groups of calbindin$^+$ Purkinje cells detected in multi-layered structures (Fig. S2C, arrowheads), possibly because of secondary effects of reduced cerebellar size.

Overall, *Ars2* deletion yielded animals with distinct cerebellar classes: a strong phenotype accompanied with loss of most granule cells and cerebellar complexity, and a weak phenotype with a mild growth defect and, surprisingly, emergence of lobule I. Previous studies have implicated that different strains of *hGFAP-Cre* exhibit different recombination patterns in the brain (Casper and McCarthy, 2006; Guo et al., 2018). Here, our observations suggest that the same *hGFAP-Cre* has varied recombination efficiency in different mice. Curiously, we were able to segregate the weak Cre-phenotype and it was inheritable for multiple generations. Thus, we primarily used this background for further studies.

Mosaic deletion of *Ars2* in NSCs permits analysis of its cell-autonomous roles

In light of phenotypic variation in the cerebellum, we assessed the variability of Cre-mediated recombination in the forebrain. We crossed *hGFAP-Cre; Ars2$^{fl/fl}$* mice with *Ai9[ROSA$^{loxP\text{-}STOP\text{-}loxP\text{-}tdTomato}$]* (Madisen et al., 2010) and monitored reporter expression (Fig. 2H). In most P0 *hGFAP-Cre; Ars2$^{fl/+}$; Ai9* mouse forebrains, tdTomato was expressed broadly (Fig. 2I). However, other brains exhibited sparse tdTomato$^+$ cells (Fig. 2J), indicating variable *Cre* expression.

Although patterns in Cre-weak brains varied across different mice, we observed consistent expression in the stratum pyramidale (SP) layer of the hippocampal CA1 region. This was accompanied by a smaller dentate gyrus (at Bregma −1.8~−2.2 mm) (Fig. 2K-M, lower panel enlargements), and a smaller hippocampal size in *hGFAP-Cre; Ars2$^{fl/fl}$; Ai9* mutants (Fig. 2M). These data suggest depleted NSC pools and/or reduced proliferation at progenitor stages (Andreu-Agullo et al., 2012). We thus focused on CA regions of these Cre-weak mice.

We next generated and validated a new polyclonal goat antibody against Ars2 C-terminal amino acids 849-863 (Fig. 2N), and analyzed Ars2 status in tdTomato$^+$ cells of CA regions of *hGFAP-Cre; Ars2$^{fl/fl}$; Ai9* mice. Indeed, immunostaining of P9 brain sections showed that Ars2 was expressed in tdTomato$^-$ SP layer neuron nuclei, but autonomously absent in Cre-activated tdTomato$^+$ clones (Fig. 2O). This highlights the *in vivo* specificity of our Ars2 antibody. Notably, *Ars2* null cells extended processes into the stratum radiatum and stratum lacunosum layers, whereas normal CA1 neurons establish connections with other neurons. Overall, the mosaic expression of *hGFAP-Cre* in hippocampal CA1 allowed direct comparison of mutant and control territories in individual animals, permitting cell-autonomous assessment of Ars2 in regulating neural development.

Ars2 is required for hippocampal neural lineage progression

The hippocampal CA area mostly contains pyramidal neurons derived from NSCs in the VZ of the hippocampal primordium (Angevine, 1965). From embryonic to early postnatal stages, these cells undergo initially vertical and then horizontal migration to form a single layer of packed excitatory neurons (Xu et al., 2014). Because the irregular pattern of DAPI-stained CA1 nuclei in *hGFAP-Cre; Ars2$^{fl/fl}$* mice (Fig. 2K′,L′) suggested defective cell migration, we characterized the identity and status of *Ars2* null cells.

The wild-type postnatal day (P)12 CA1 region is composed of post-mitotic neurons, as indicated by lack of bromodeoxyuridine (BrdU) incorporation. *Ars2* knockout regions similarly lack BrdU$^+$ cells, indicating they did not aberrantly retain mitotic cells (Fig. 3A). On the other hand, these clones failed to express NeuN (Rbfox3), indicating that *Ars2* mutant cells cannot differentiate into mature excitatory neurons (Fig. 3B), indicating a late defect.

As summarized in Fig. 3C, NSCs undergo consecutive developmental stages before differentiating into mature neurons. In the dorsal forebrain, where the hippocampus resides, NSCs or radial glia are first specified into proliferative IPCs (neuroblasts). IPCs then exit the cell cycle and become immature neurons expressing DCX (Gleeson et al., 1999) and TBR1; note TBR1 is expressed in some types of mature cortical neurons but is very low in mature CA neurons (Englund et al., 2005). Immature neurons then undergo terminal differentiation and develop into NeuN$^+$ mature neurons. Furthermore, the Notch corepressor BEND6 represents an early marker of post-mitotic immature neurons that is broadly maintained by mature neurons (Dai et al., 2013a). We observed accumulation of both DCX and TBR1 in *Ars2* mutant cells in P12 brain CA1, whereas these markers were poorly expressed in neighboring Ars2$^+$ regions (Fig. 3D,E). Furthermore, *Ars2* null cells expressed high levels of BEND6 (Fig. 3F). The absence of NeuN, along with the presence of DCX, TBR1 and BEND6, indicated that *Ars2* knockout cells arrest at early postmitotic neuronal stages. In addition, *Ars2-cKO* CA1 regions exhibit astrogliosis, as indicated by the astrocyte marker GFAP (Fig. S3).

Beyond cell identity analyses, we observed sporadic activation of caspase 3 specifically within *Ars2*-null clusters (Fig. 3G), indicating that *Ars2* deletion also triggers apoptosis. Although we did not previously observe excess cell death upon *Ars2-cKO* in adult SVZ (Andreu-Agullo et al., 2012), increased apoptosis during embryonic development may contribute to reduced hippocampal size of Cre-weak *Ars2-cKO* mice.

Together, these data extend the role of Ars2 from NSC self-renewal to governing terminal differentiation within the neuronal lineage in CA1. Interestingly, these experiments suggest that Ars2, which has multiple substantial RNA-processing activities, is not essential for early neuronal fate commitment.

Ars2 is continuously required for adult neurogenesis in the hippocampus

Beyond the embryonic VZ and adult SVZ, the DG SGZ is the third NSC niche in the mouse forebrain. To investigate whether Ars2 regulates SGZ NSC development, we first characterized its expression pattern in the DG. Immunostaining of 2-month-old mouse brains revealed expression of Ars2 in adult NSCs, marked by double positivity for GFAP and SOX2 (Fig. 4A). Many DCX$^+$ neuroblasts appeared to downregulate Ars2 (Fig. 4B, asterisks), whereas most NeuN$^+$ mature neurons expressed Ars2 (Fig. 4C). Thus, the expression dynamics of Ars2 are similar between embryonic (Fig. 1) and adult neural lineages.

Development (2020) 147, dev180018. doi:10.1242/dev.180018

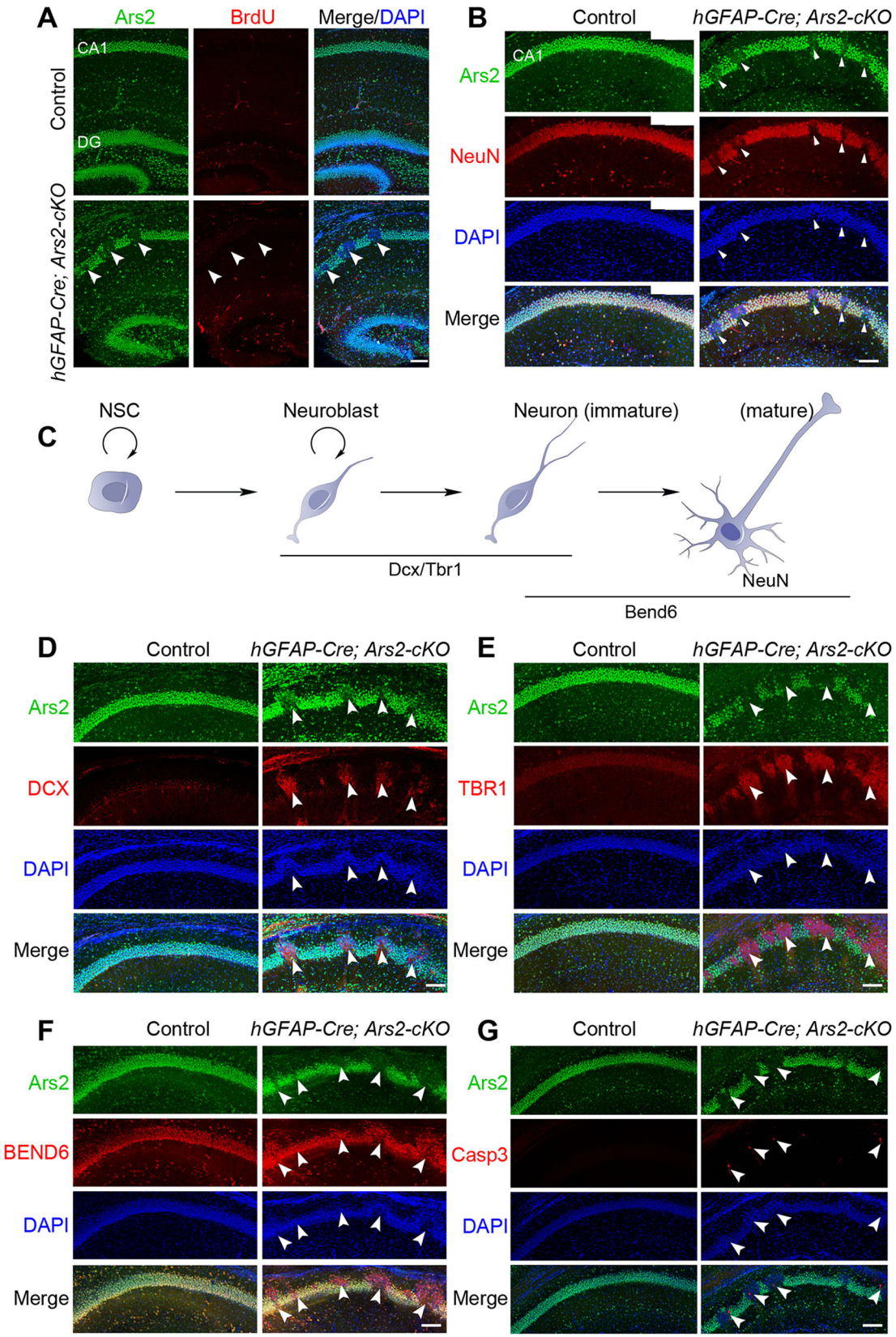

Fig. 3. Ars2 is required for neuronal maturation but not for neuronal specification. (A) P12 control (*hGFAP-Cre; Ars2*$^{fl/+}$) and *hGFAP-Cre; Ars2*$^{fl/fl}$ brains immunostained for Ars2 (green), BrdU (red) and DAPI (blue). DG, dentate gyrus. (B) P12 brain immunostained for Ars2 (green), NeuN (red) and DAPI (blue). *Ars2*-knockout hippocampal pyramidal cells (arrowheads) fail to differentiate into mature neurons. (C) Summary of neural development and stage-specific molecular markers. (D-F) P12 hippocampal CA1 region demonstrates that *Ars2*-knockout cells inappropriately maintain neuroblast/newborn neuronal markers DCX (D) and TBR1 (E), and express BEND6 (F). (G) Immunostaining for cleaved caspase-3 (red) reveals sporadic cell death preferentially in *Ars2* null regions. Arrowheads indicate mosaic *Ars2*-knockout regions in the hippocampal stratum pyramidal layer. Scale bars: 100 µm.

Development (2020) 147, dev180018. doi:10.1242/dev.180018

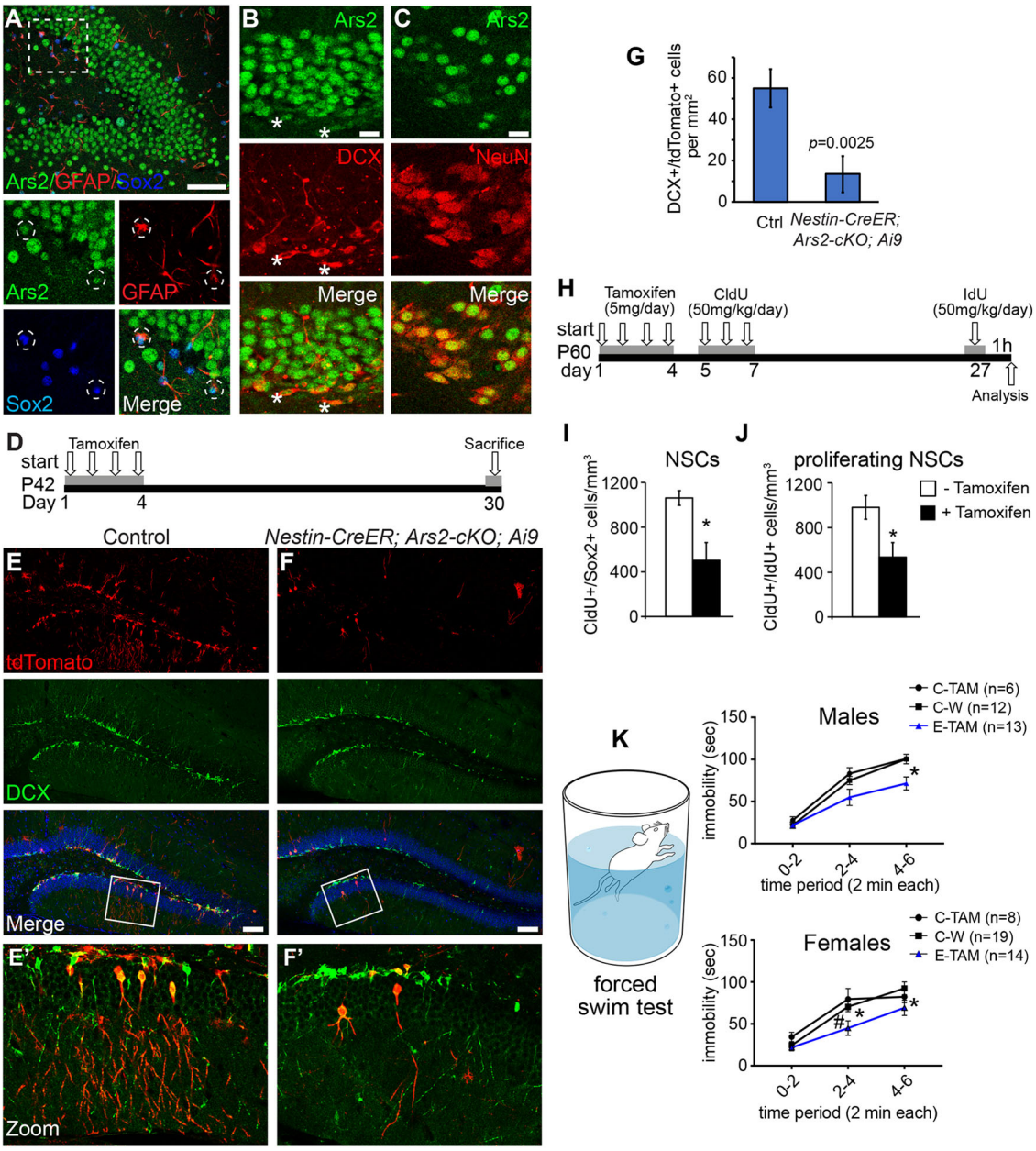

Fig. 4. Ars2 is required for adult neurogenesis and select behavioral functions. (A) Immunostaining of adult dentate gyrus (DG). Bottom panels show magnification of boxed area, which indicates a SOX2$^+$ cell with low Ars2. Dashed circles indicate co-localization of Ars2 (green), SOX2 (blue) and GFAP (red). (B) Adult DG shows co-localization of Ars2 (green) and DCX (red), but Ars2 is downregulated in some DCX$^+$ cells (marked with asterisks). (C) Adult DG shows co-expression of Ars2 (green) and NeuN (red). (D) Scheme of tamoxifen administration in *Nestin-CreERT2; Ai9; Ars2$^{fl/fl}$* mice. (E-F′) Reduction of immature DG neurons co-expressing DCX (green) and tdTomato (red) in *Nestin-CreERT2; Ars2$^{fl/fl}$; Ai9* mice compared with control littermates. E′ and F′ show magnifications of the boxed areas in E and F, respectively. (G) Quantification of E,F; n=3, two tailed t-test; data are mean±s.d. (H) Experimental scheme of proliferating NSC quantification assay used in J and K. (I,J) Quantitative evaluation of CldU$^+$/SOX2$^+$ NSCs and CldU$^+$/IdU$^+$ proliferating NSCs in the DG of control and induced *cKO* mice. *P<0.05. n=3, two-tailed t-test; data are mean±s.e.m. (K) Reduced immobility time of both male and female Ars2-CKO mice. C-TAM, control *Ars2$^{fl/fl}$* injected with TAM; C-W, control wild type; E-TAM, *Cre$^+$ Ars2$^{fl/fl}$* injected with TAM. Repeated measures of ANOVA. Males: group effect F(2, 32)=4.449, P=0.0197; group×time interaction F(4, 64)=2.63, P=0.0424; multiple t-test with the Holm-Sidak method; C-W versus E-TAM *P=0.0081. N=6, 12, 13. Females: group effect F(2, 38)=4.08, P=0.0248; C-W versus E-TAM *P=0.0237 and 0.0306; C-TAM versus E-TAM $^{\#}P$=0.0179. N=8, 19, 14. Scale bars: 50 µm in A-C; 100 µm in E,F.

To investigate the function of Ars2 in specification and differentiation of adult DG NSCs, we utilized *Nestin-CreERT2* to conditionally delete *Ars2* in a tamoxifen-dependent manner. To test the efficacy of this system, we generated triple-transgenic mice bearing *Ai9* to monitor Cre-mediated activation of tdTomato. We examined neurogenesis one month after tamoxifen administration at 6 weeks of age (four daily doses) by immunostaining DCX to mark neuroblasts and tdTomato to monitor Cre activity (Fig. 4D). The number of tdTomato$^+$ cells expressing DCX decreased dramatically in *Nestin-CreERT2*; *Ai9*; *Ars2$^{fl/fl}$* mice (Fig. 4E-G), indicating that Ars2 maintains adult neurogenesis. In addition, the remaining DCX and tdTomato co-labeled cells showed reduced numbers and lengths of neural processes.

Development (2020) 147, dev180018. doi:10.1242/dev.180018

To test the role of Ars2 in generating adult SGZ NSCs, we administered four doses of tamoxifen to two-month-old *Nestin-CreERT2*; *Ars2*$^{fl/fl}$ animals, then injected chlorodeoxyuridine (CldU) to monitor the fate of proliferating cells over 3 weeks, and iododeoxyuridine (IdU) 1 h before sacrifice to label actively proliferating cells (Fig. 4H). Compared with control animals without tamoxifen treatment, conditional ablation of *Ars2* resulted in substantial loss of label-retaining SOX2$^+$ cells (i.e. quiescent NSCs), as well as CldU$^+$/IdU$^+$ cells (i.e. proliferating NSCs) in adult SGZ (Fig. 4I,J). We conclude that Ars2 is essential for normal levels of ongoing adult neurogenesis and neuroblast generation in the fully mature DG.

Deletion of *Ars2* in SGZ NSCs causes abnormal stress coping

The possibility to obtain temporally selective deletion of *Ars2* in adult SVZ allowed us to study its impact on adult behaviors. First, we confirmed that adult-specific ablation of Ars2 in tamoxifen-treated *Nestin-CreERT2*; *Ars2*$^{fl/fl}$ (i.e. *Ars2-cKO*), beginning at two months, resulted in substantial reduction in DCX$^+$ staining four weeks later and thus a deficit in adult neurogenesis (Fig. S4). Although precise functions of adult-born granule cells remain controversial, loss- and gain-of-function studies suggest their involvement in cognitive functions and emotional behavior, including spatial learning/memory (Blaiss et al., 2011; Dupret et al., 2008), contextual fear learning (Saxe et al., 2006), stress responsiveness (Jedynak et al., 2014) and anxiety (Revest et al., 2009).

After determining that *Ars2-cKO* did not substantially affect overall levels of locomotion (Fig. S5A), we tested these mice for cognitive performance. We employed two paradigms for hippocampal-dependent learning and memory: the Morris water maze (MWM) and contextual fear conditioning (CFC). The MWM test is a spatial task to navigate a water-filled pool, using distal room cues, to find and memorize the location of a submerged escape platform. Following repeated learning trials, the platform is removed and mice are tested to see whether they recall the platform location by spending more time in the corresponding area of the maze. CFC is an associative learning paradigm that tests the ability of mice to link an adverse event (footshock) to the corresponding context or environment, to anticipate the event when exposed to the context later. One or a few context-footshock associations suffice to elicit anticipatory freezing to context exposure alone. *Nestin-CreERT2*-mediated *Ars2-cKO* in adult mice did not cause deficits in either cognitive tests (MWM or CFC, Fig. S5B,C), indicating no impairments in hippocampal spatial and associative memory.

We next tested responses to fear- and anxiety-inducing stimuli. In the elevated plus maze (EPM), mice tend to avoid the two open and elevated arms and prefer the two closed protected arms. The relative time spent in open versus open+closed arms quantifies fear response. In the forced swim test (FST), mice exhibit vigorous escape-directed behavior (swimming and climbing) when placed in a water-filled beaker, an inescapable environment. The time of immobility (i.e. no swimming and climbing) is quantified over three 2-min intervals after placing mice in the beaker. Although reduced immobility in FST was originally used to predict antidepressant-like activity (Porsolt et al., 1978), this has more recently been interpreted as increased active coping to inescapable stress. We observed that avoidance of open EPM arms was not substantially altered in *Ars2-cKO* mice, suggesting normal responses in this relatively low and avoidable stress environment (Fig. S5D). By contrast, *Ars2-cKO* mice (Cre$^+$, TAM) exhibited reduced immobility (i.e. increased swimming/climbing) in the FST (Fig. 4K), suggesting increased responsiveness to a strong and inescapable stress. Importantly, both male and female *Ars2-cKO* mice exhibited FST behavioral differences relative to control *Nestin-CreERT2; Ars2*$^{fl/fl}$ mice that were sham-treated, as well as to control *Nestin-CreERT2; Ars2*$^{fl/+}$ mice treated with tamoxifen. Thus, increased stress responsiveness of *Ars2-cKO* mice was robust to sex and is not attributable to tamoxifen, genotype or stress associated with prior experimental handling.

Overall, these data indicate that defects in adult neurogenesis caused by *Ars2-cKO* manifest with specific behavioral consequences. They do not alter cognitive functions or the ability to cope with a low stress environment, but yield specific defects in coping with inescapable stress.

Ars2 broadly associates with enhancers selectively in NSCs

Following these cellular and functional assays, we sought insights into molecular roles of Ars2. We have reported that Ars2 binds to *Sox2* regulatory regions and transcriptionally activates *Sox2* during NSC renewal, and used neurosphere cultures as a model (Andreu-Agullo et al., 2012). To extend a genomic view, we generated Ars2 and IgG ChIP-seq data from self-renewing primary neurospheres cultured from adult SVZ (Fig. S6A). Indeed, the previously identified enhancers upstream of *Sox2* were strongly targeted by Ars2 (Fig. 5A) and comprised some of the most enriched regions genomewide.

As Ars2 has extensive roles in RNA biogenesis, Ars2 might associate with chromatin indirectly through RNA or RNA synthesis machinery. We therefore generated additional ChIP-seq data using RNase-treated sonicated material. Inspection of *Sox2* showed that strong Ars2 peaks at its 5′ UTR/3′ UTR were selectively lost following RNase treatment, whereas Ars2 peaks at *Sox2* enhancers remained (Fig. 5A). These data are consistent with the notion that RNase treatment disrupted transcript-associated Ars2 tethering to chromatin.

The Ars2 ChIP peaks at *Sox2* were so abundant that some individual Ars2 ChIP-seq reads at *Sox2* were highly duplicated (up to millions of reads out of 100-180M reads). The *Sox2* peaks did not resemble classical PCR artifacts as they had smooth contours (Fig. 5A), instead of square blocks of single amplified reads. However, as we did not use unique molecular identifiers during library construction, we were conservative and removed duplicate reads for peak-calling. Even when considering only unique reads, *Sox2* enhancer peaks remained highly enriched compared with IgG ChIP-seq. The peaks (≥10 reads, ≥2.5 fold compared with IgG control) were then subtracted using the mouseENCODE blacklist. Using these parameters, we obtained 13,703 regions in Ars2 ChIP-seq data without RNase (Fig. 5B). Fewer peaks were identified in RNase-treated Ars2 ChIP-seq data (6327), but the strong majority of these (4459 peaks) were shared with Ars2 ChIP-seq data generated without RNase treatment (Fig. 5B).

When stratifying overlaps by ChIP peak strength, it was evident that common peaks were concentrated amongst higher-enriched Ars2 peaks in the respective ChIP-seq datasets (Fig. 5C). In addition, we observed genomewide reduction of transcription start site (TSS)-associated peaks in RNase-treated Ars2 ChIP data, compared with data without RNase treatment (Fig. 5D). We took the common peaks between the Ars2 ChIP datasets to represent confident RNase-independent chromatin association of Ars2, and used these for downstream analyses.

To verify these ChIP data, we selected regions with different levels of Ars2 enrichment, along with negative controls, for ChIP-

Development (2020) 147, dev180018. doi:10.1242/dev.180018

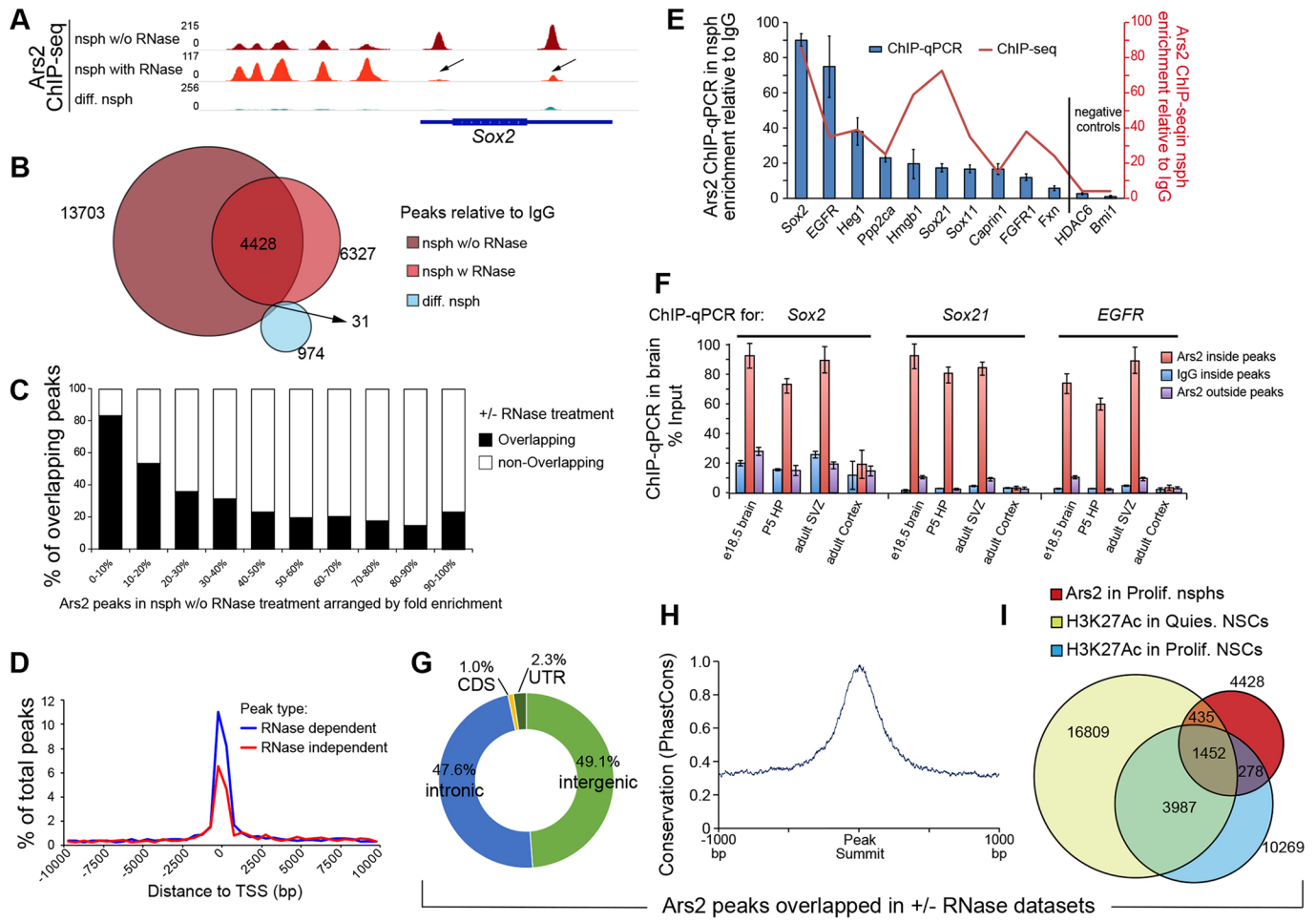

Fig. 5. Ars2 broadly associates with enhancers selectively in NSCs. (A) Ars2 ChIP-seq data were collected from self-renewing neurospheres (nsph), a model for NSCs, and following their differentiation (diff. nsph). Libraries were made ±RNase treatment. Representative data are shown at *Sox2*, a previously characterized Ars2 target. Its 5′ UTR/3′ UTR peaks are RNA dependent, whereas its enhancer peaks are RNase independent. Furthermore, limited binding is observed in ChIP-seq from differentiated neurospheres. Arrows indicate Ars2 peaks located on *Sox2* 5′UTR and 3′UTR, which disappear after RNase treatment. (B) Venn diagram summarizes Ars2 peak overlaps in NSCs without RNase treatment, NSCs with RNase treatment and differentiated neurospheres. (C) Classification of overlaps between Ars2 ChIP ±RNase treatment by ChIP peak strength. The overlaps are greater amongst highest-bound peaks. (D) Ars2 peaks near transcription start sites (TSS) were reduced after RNase treatment. (E) ChIP-qPCR validation across a range of Ars2 associations in NSCs. *HDAC6* and *Bmi1* had minimal binding in ChIP-seq data, serving as negative controls. We observed general concordance between ChIP-seq and ChIP-qPCR data. Data are mean±s.e.m. (F) Representative NSC genes (e.g. *Sox2*, *Sox21* and *Egfr*) were validated by ChIP-qPCR using mouse tissue. Compared with ChIP from adult cortex, strong enrichment was observed in NSC-containing tissues. Data are mean±s.e.m. (G) The vast majority of Ars2 common peaks locate in intronic (47.6%) and intergenic (49.1%) regions. (H) Ars2 peaks are locally conserved. The *y*-axis shows PhastCons values aggregated for 4428 common NSC Ars2 peaks. (I) Venn diagram shows the genome-wide overlaps between 4428 common Ars2 and active enhancer marker H3K27Ac in NSCs.

qPCR tests. Overall, we obtained good concordance between ChIP-Seq and ChIP-qPCR from neurospheres (Fig. 5E). Furthermore, we performed ChIP-qPCR of Ars2 peaks at *Sox2*, *Sox21* and *Egfr* using mouse forebrain tissues at different developmental stages. In tissues containing NSCs, such as embryonic day (E)18.5 brain, P5 hippocampus and adult SVZ, these Ars2 ChIP-seq regions confirmed enrichment compared with IgG ChIP and adjacent ChIP-seq signal-negative sites. In contrast, ChIP-qPCR using adult cortex, which consists of post-mitotic neurons and glial cells, showed no ChIP enrichment (Fig. 5F).

To explore whether Ars2 has dynamic chromatin interactions, we performed Ars2 ChIP-seq from differentiated neurospheres, which include early post-mitotic neurons, astrocytes and oligodendrocytes (Fig. S6B). Although we obtained >104 M reads mapped to the mm10 genome, we obtained only 974 peaks (Fig. 5B). Moreover, although not included in the mouse ENCODE genomic blacklist, many of these peaks located in non-conserved regions, unassembled genomic regions and Y chromosome (Fig. S6C). Interestingly, *Cwc22* exhibited intense Ars2 binding in differentiated neurospheres (Fig. S6C). Only 31 peaks were co-targeted by Ars2 in proliferating NSCs, most of which were also not conserved (Fig. 5B; Fig. S6D). This is consistent with our finding that Ars2 is poorly expressed by immature neurons and that *Ars2* knockout NSCs can progress into premature neuronal stages.

Although analyses centered on TSS give an impression of centered Ars2 enrichment close to basal promoters (Fig. 5D), its RNA-independent chromatin-associated regions mostly comprise intronic or intragenic regions distal from TSS, with ChIP sites in CDS and UTRs accounting for only 1% and 2.3% of total peaks, respectively (Fig. 5G; Fig. S6D,E). Still, Ars2 preferentially associated with evolutionarily conserved regions, as its ChIP-seq peaks coincide with local maxima in pan-mammalian PhastCons scores (Fig. 5H).

Development (2020) 147, dev180018. doi:10.1242/dev.180018

To further evaluate whether Ars2 is located in active regulatory elements in NSCs, we compared Ars2 peaks with ChIP-seq data for the active enhancer-associated mark H3K27ac (Martynoga et al., 2013) and the promoter-associated mark H3K4me3 (Benayoun et al., 2014). We observed that 2165/4459 Ars2 NSC peaks (48.6%) overlapped with H3K27Ac-marked enhancers in the two NSC states (1887 in proliferating NSCs and 1730 in quiescent NSCs). Most of these regions (1452, 67.1%) were identified in both quiescent and proliferating cells (Fig. 5I). In contrast, only 971 of the 4459 peaks (21.8%) were marked by H3K4me3 (Fig. S6F). These analyses suggest that Ars2-bound regions are more likely to be intronic and intragenic enhancers in NSCs, and that substantial Ars2-DNA interactions are independent of co-transcriptional associations via RNA. Overall, these ChIP-seq data broadly extend the notion that Ars2 associates with enhancers in a temporally dynamic fashion in NSCs.

Ars2 targets many neural regulators

Many known NSC regulators were bound by Ars2 in both datasets. Besides *Sox2*, these included genes such as *Nes*, *EGFR and Ascl1* (Fig. S6; Fig. 6). Moreover, gene ontology (GO) analysis revealed that Ars2 targets are enriched for NSC and brain development functions (Fig. 6A), including *Hes1*, *Hes5* and *Notch1* (Fig. 6B). Functional categories related to myelinating glial development were also significantly enriched, such as *Olig1/2* (Fig. 6B). ChIP-seq analysis revealed that these genes are bound by Ars2 only in NSCs but not in differentiated neurospheres. In contrast, there was no ChIP enrichment at *Bend6*, *Tbr1* or *Dcx* (Fig. S6G), genes with a maintained expression in *Ars2-cKO* mosaic tissue (Fig. 3D-F).

We performed additional ChIP-qPCR validations using RNase-treated material and our new Ars2 antibody, which our cKO stainings showed to be specific for endogenous Ars2 (Figs 2 and 3). Compared with IgG ChIP and a negative control region from *Sox2*, we confirmed Ars2 enrichment at *Hes5*, *Notch1* and *Olig1/2* (Fig. 6C). Given that Ars2 associates with active enhancers, we next assessed how Ars2 loss impacts target expression. We have previously used *Ars2-shRNAs* in adult NSCs (Andreu-Agullo et al., 2012), but here used Cre virus to delete the floxed *Ars2* allele in embryonic NSC cultures (Fig. 6D). We observed downregulation of direct Ars2 targets *Hes1*, *Hes5* and *Sox2* in qPCR assays (Fig. 6D). Although we recognize that loss of any factor crucial for NSC maintenance might lead to indirect changes in gene expression due to alteration of cell identity, these data support the notion that Ars2 can regulate bound loci in NSCs.

We extended our *in vitro* assessments to *in vivo* settings. To circumvent the varied knockout efficiency and hydrocephalus by *hGFAP-Cre*, we crossed $Ars2^{fl/fl}$ mice to *Olig2-Cre*, which stably expresses Cre in a subset of NSCs that give rise to oligodendrocytes, interneurons (Fig. 6E) and motor neurons. As *Olig2-Cre;* $Ars2^{fl/fl}$ mice die at P0, possibly owing to failure of motor neuron genesis, we focused on embryonic stages. At E15.5, *Olig2-Cre* recombination is constrained to the ventral VZ, which gives rise to adult SVZ and ventral originating oligodendrocyte precursors (OPCs), but it is not active in dorsal neural progenitors (Fig. 6E). Immunostaining of *Olig2-Cre;* $Ars2^{fl/fl}$ medial ganglionic eminence (MGE) showed reduced thickness and reduction of dividing markers (Ki67 and BrdU, Fig. 6F). Defective ventral proliferation was consistent with the requirements of Ars2 for adult SVZ (Andreu-Agullo et al., 2012) and embryonic forebrain NSC development (Fig. 1C). In contrast, there were no proliferation defects in the dorsal VZ, in which *Olig2-Cre* is not yet active (Fig. S7). We further observed that in E15.5 *Olig2-Cre;* $Ars2^{fl/fl}$ MGE, cells negative for Ars2 reliably lacked SOX2, consistent with their regulatory relationship (Fig. 6G). These observations support the requirement of Ars2 in NSCs.

Ars2 exhibits broad genomic co-binding with core NSC factor SOX2

To interpret the ChIP-seq data within broader regulatory networks, we performed *de novo* motif discovery. Amongst the top 4000 Ars2 peaks were consensus sequences for known transcription factors (TFs). These included high frequency (1148/4000 regions, *E*=1.6e-62) of class II bHLH activator sites, which closely resemble the recently defined consensus for Ascl1 (Casey et al., 2018), a well-known neural lineage specification TF (Guillemot et al., 1993). Other motifs included those for NRF1 (641/4000, *E*=4.0e-140), an activator of NMDA receptor genes in neurons (Dhar and Wong-Riley, 2009); EGR1 (1347/4000, *E*=1.2e-69), an immediate early gene of active NSCs (Llorens-Bobadilla et al., 2015) that mediates NSC expansion upon hypoxia (Alagappan et al., 2013); and NFIX (989/4000, *E*=1.7e-62), a TF crucial for NSC quiescence (Martynoga et al., 2013).

The only unknown motif identified was GCGTGCGT, the second most significant motif (384/4000, *E*=1.0e-169) (Fig. S8). However, this did not resemble the sequence we have previously characterized in *Sox2* to associate with Ars2 (Andreu-Agullo et al., 2012), even though this region was indeed strongly enriched in our ChIP-seq data. To further evaluate the Ars2 binding site in the *Sox2* regulatory region, we performed gel shift analysis using a minimal 27 bp region that bound *in vitro* translated Ars2. By testing probes bearing clustered mutations that tiled across its length, we identified specific nucleotides necessary for Ars2 association to DNA *in vitro* (Fig. S9). However, we are not presently able to relate the nucleic acid binding properties of Ars2 to ChIP motifs. Thus, it appears Ars2 ChIP-seq data may represent mostly indirect (albeit RNA-independent) associations with chromatin.

The most intriguing aspect of Ars2 ChIP-seq data regarded the top-enriched motif. This was present in 73/100 top Ars2-ChIP peaks (*E*=6.4e–41) (Fig. 7A,B), and was the most highly represented motif in all other peak classes, although more strongly enriched amongst top Ars2-ChIP peaks (Fig. 7B; Fig. S8). According to the JASPAR TF database, this motif resembles the consensus recognized by SOX2 (Matrix ID: MA0143.3, *E*=1.87e-08) (Fig. 7A), a well-established NSC transcription factor that is targeted by Ars2 during NSC development.

The SOX2 motifs are located near Ars2 peak summits (Fig. 7C), suggesting close association. To evaluate colocalization of Ars2 and SOX2 genomewide, we performed SOX2 ChIP-seq in proliferating NSCs, which identified 3881 peaks (Fig. 7D). *De novo* motif discovery identified the known Sox2 motif as the most highly enriched DNA consensus sequence in SOX2-ChIP peaks, validating data quality. GO analysis of SOX2-associated genes showed enriched functions relating to brain development and inhibition of neuronal differentiation (Fig. 7E). Strikingly, 1500/3881 SOX2 peaks were co-occupied by Ars2 (Fig. 7D), providing evidence for broad colocalization of these factors on chromatin. Interestingly, SOX2 motif enrichment was slightly stronger amongst SOX2 peaks co-bound with Ars2 (Fig. 7F).

Inspection of ChIP tracks confirmed co-occupancy of Ars2 and SOX2 at many NSC loci, including *Hes5*, *Notch1* and *Olig1/2* enhancers (Fig. 6C), as well as *Sox2*, *Ascl1* and *EGFR* (Fig. 7G). As we had confirmed these for Ars2 binding by ChIP-qPCR, we selected these loci for SOX2 ChIP-qPCR using RNase-treated chromatin samples. These assays confirmed that SOX2 associates

Development (2020) 147, dev180018. doi:10.1242/dev.180018

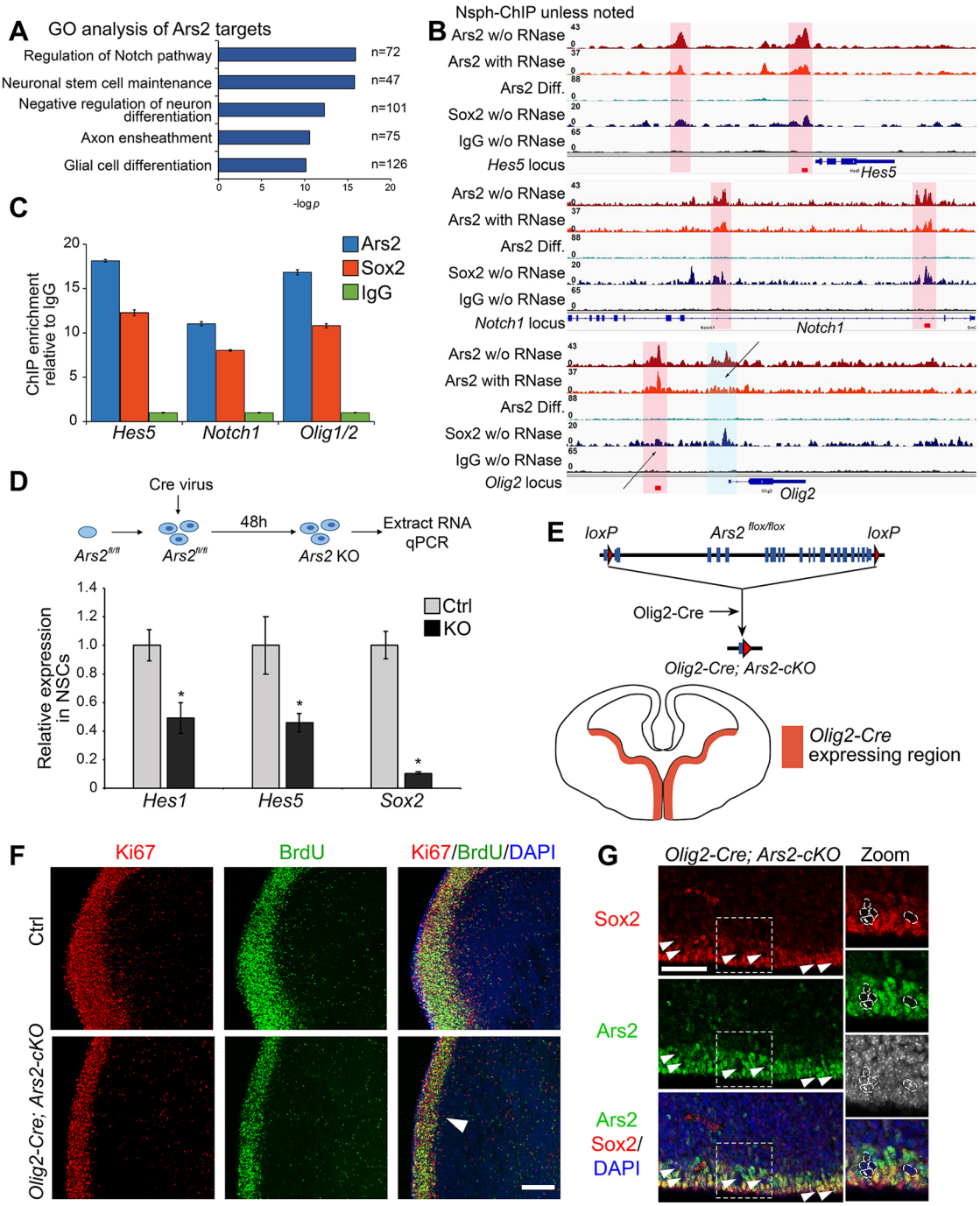

Fig. 6. Ars2 targets essential neural regulators. (A) Functional annotation of Ars2-bound regions in proliferating NSCs. (B) Ars2 and SOX2 enrichment profiles at representative NSC regulators (e.g. *Hes5* and *Notch1*) and glial regulator *Olig2*. (C) Selected Ars2 peaks were validated by ChIP-qPCR (red bars in panel B indicate amplicon sites) with our independent Ars2 antibody; i.e. different from the one used for Ars2 ChIP-seq. SOX2 ChIP-qPCR indicates genomic colocalization. Experimental material was treated with RNase before PFA fixation and ChIP. Data are mean±s.e.m. (D) Schematic of Cre-virus infection strategy and qPCR measurements of NSC genes (e.g. *Hes1*, *Hes5* and *Sox2*) from primary *Ars2*$^{flox/flox}$ NSCs 48 h after Cre-virus infection. Data are mean±s.e.m. Hes1 P=0.0053; Hes5 P=0.0140; Sox2 P=0.0001; two-tailed t-test applied; data are mean±s.e.m. (E) Strategy to knockout *Ars2* in embryonic ventral NSCs using *Olig2-Cre*. Red region in the diagram indicates *Olig2-Cre*-expressing area in embryonic ventral forebrain. (F) E15.5 *Olig2-Cre; Ars2*$^{fl/+}$ (ctrl) and *Olig2-Cre; Ars2*$^{fl/fl}$ medial ganglionic eminence (MGE) region stained for Ki67 (red), BrdU (green) and DAPI (blue). Arrowhead indicates that the thickness of MGE, the ventral progenitor region, is reduced in mutants. (G) E15.5 *Olig2-Cre; Ars2*$^{fl/fl}$ ventral VZ stained for SOX2 (red), Ars2 (green) and DAPI (blue). Arrowheads indicate that cells without Ars2 are specifically negative for SOX2. Panels on the right show magnification of the boxed areas on the left. Scale bar: 100 µm in F; 50 µm in G.

with these Ars2-bound loci (Figs 6C and 7H). Nevertheless, despite strong trends for co-association, some regions were individually bound by Ars2 or SOX2. For example, *Hes1*, *Pou3F2* and *Myt1l* were bound only by Ars2 (Fig. S10A-C), whereas *Gli2*, *Has2* and *Zcchc2* were only identified with SOX2-ChIP peaks (Fig. S10D-F). Thus, these factors exhibit specificity in their respective ChIP-seq datasets. Overall, although ChIP-seq data did not resolve whether Ars2 directly associates with chromatin via a distinct DNA binding

Development (2020) 147, dev180018. doi:10.1242/dev.180018

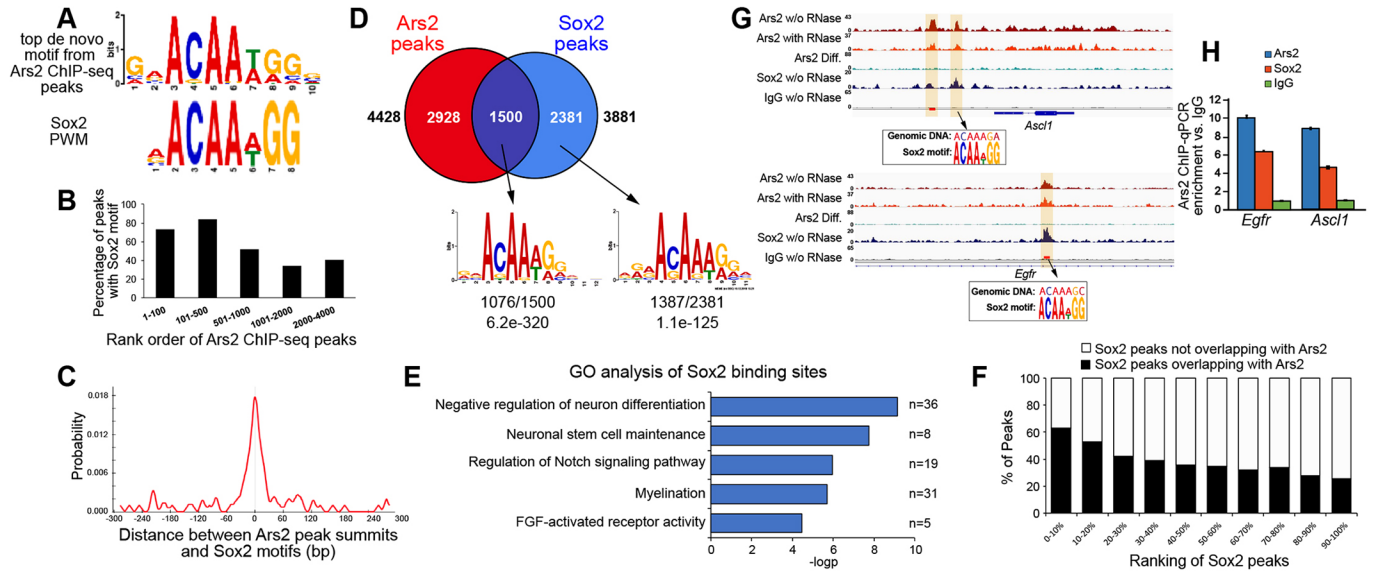

Fig. 7. Ars2 exhibits broad genomic co-localization with NSC factor SOX2. (A) *De novo* motif analysis of Ars2 ChIP peaks identified a SOX2/3/6 consensus as the top enriched motif. (B) The SOX2 motif is highly represented in all categories of Ars2-bound regions classified by ChIP-seq enrichment, but especially enriched amongst highest-ranked Ars2 peaks. (C) SOX2 motifs are located close to Ars2 peak summits. (D) SOX2 ChIP-seq data was generated from neurospheres, and overlap analysis of peak calls reveals broad co-localization between SOX2 and Ars2. (E) GO analysis of SOX2 bound regions. (F) Overlap analysis of SOX2 and Ars2 peaks shows enrichment of co-binding amongst the stronger SOX2 peaks. (G) Distribution of Ars2 and SOX2 at representative NSC genes, *Ascl1* and *Egfr*, in proliferating and differentiated neurospheres. The JASPAR SOX2 motif and corresponding sequence are shown. (H) Ars2 and SOX2 co-targeting regions were validated by ChIP-qPCR (red bars in panel G indicate amplicon sites) with our independent Ars2 antibody, i.e. different from the one used for Ars2 ChIP-seq. Materials were treated with RNase before PFA fixation and ChIP. Data are mean±s.e.m.

site, we reveal unexpected genomic co-association of Ars2 and SOX2, two factors needed for NSC self-renewal.

DISCUSSION

Stage-specific requirements of Ars2 during neural development

Ars2 is well-established as an RNA-processing factor, and interacts with diverse RNA machineries to regulate multiple transcript types (Andersen et al., 2013; Gruber et al., 2009; Hallais et al., 2013; Sabath et al., 2013; Sabin et al., 2009; Wang et al., 2018). Thus, Ars2 is intuitively considered as a ubiquitous protein with housekeeping functions. Here, our systematic conditional knockout experiments yield unanticipated stage-specific roles for Ars2 during neural development. Ars2 has cell type-specific expression in neuronal lineages and not only maintains NSCs, but also controls post-mitotic neuron maturation. In the adult, hippocampal Ars2 is crucial for adult neurogenesis in the DG, and required for specific aspects of emotional but not cognitive behavior. Thus, Ars2 has dynamic roles in neuronal lineages.

Broad chromatin localization of Ars2 to enhancers in NSCs

Studies of *Sox2* enhancers identified an unconventional role of Ars2 as a transcriptional regulator (Andreu-Agullo et al., 2012). Here, we used ChIP-seq to reveal that Ars2 associates broadly with chromatin in a cell type-specific manner. Ars2 is a nuclear co-transcriptional RNA processor (Schulze and Cusack, 2017). However, beyond association to actively transcribed exons, we defined thousands of RNase-independent Ars2 ChIP peaks, which exhibit genomic features of enhancers.

How does Ars2 interact with DNA? A limitation of our current Ars2 ChIP analysis is that it did not reveal a direct binding site consensus, which was sought from a previous study (Andreu-Agullo et al., 2012). Ars2 structural analyses (Schulze et al., 2018) revealed how the Ars2 RRM domain and C terminus interact with RNA and protein partners, but we know less about the rest of Ars2, including the RDEGP-rich N terminus, the domain of unknown function 3546 (DUF3546), the middle helical core and the C-terminal leg. Perhaps structural data can provide insights into its association with DNA. However, an intriguing observation is that Ars2 RNase-independent ChIP peaks in NSCs are highly enriched for SOX2 motifs, and SOX2 ChIP-seq confirmed broad colocalization of Ars2 and SOX2 in NSCs. Because SOX2 primes a permissive chromatin landscape in the NSCs during SGZ neurogenesis (Amador-Arjona et al., 2015), Ars2 might be recruited by SOX2 to DNA. Although studies of FLAG-SOX2 pulldown from E11.5 cortex did not recover Ars2 (Engelen et al., 2011), it is tempting to speculate a feed-forward loop, whereby *Sox2* is not only targeted by Ars2, but Ars2 has a broader role in working with SOX2 at NSC enhancers.

Arabidopsis Ars2 ortholog SERRATE processes miRNAs by physically interacting with the SWI2/SNF2 complex (Wang et al., 2018). Mammalian Ars2 contains all functional domains of *Arabidopsis* SERRATE, and SWI/SNF also plays crucial roles during mammalian neurogenesis. Similar to the role of Ars2 in neural specification, the SWI/SNF complex is not required for the specification of neural progenitors into OPCs and does not associate with DNA in OPCs. More interestingly, SWI/SNF null OPCs [cKO of SWI/SNF core ATPase Brg1 (Smarca4)] cannot differentiate and undergo apoptosis (Yu et al., 2013), which we also observed in Ars2 null early-born neurons. Further studies can address whether NSC Ars2 functions with SWI/SNF or other chromatin remodeling/modifying complexes.

Impact of newly-born neurons on behavior

The contribution of adult-born neurons in the DG to cognitive and emotional behaviors has been extensively studied by impairing

Development (2020) 147, dev180018. doi:10.1242/dev.180018

adult neurogenesis using genetic manipulations, focal irradiation or chemical tools. Perhaps because of differences across these approaches, their effectiveness and side effects, these studies collectively yielded inconsistent findings. Similar to our observations with *Ars2-cKO* mice, most studies found no effect of suppressing adult DG neurogenesis on spatial memory in the MWM (Groves et al., 2013; Jaholkowski et al., 2009; Saxe et al., 2006). However, one study reported a cognitive deficit in a macrophage migration inhibitory factor-deficient model (Conboy et al., 2011). Although several studies conclude that loss of adult-born neurons impairs contextual fear conditioning responses (Deng and Gage, 2015; Saxe et al., 2006), some, including this report with *Ars2-cKO* mice, found normal fear memories in mice with impaired adult neurogenesis (Drew et al., 2010). Behavior in the FST is even more variable, with different strategies of impairing adult neurogenesis reported as reducing (Jedynak et al., 2014), increasing (Snyder et al., 2011) or causing no change (Deng and Gage, 2015; Revest et al., 2009) to immobility behaviors. We note that the reduced immobility behavior, interpreted as increased stress responsiveness, of *Ars2-cKO* mice is similar to the behavior of *cyclin D2-cKO* mice in the FST (Jedynak et al., 2014). Finally, reduced neurogenesis in *Ars2-cKO* mice caused no anxiety in a low stress and escapable situation, represented by the open arm of the EPM, similar to some models (Deng and Gage, 2015; Jedynak et al., 2014), whereas other models exhibited increased anxiety-like behavior (Conboy et al., 2011; Revest et al., 2009).

Considering these diverse behavioral conclusions from different models of compromised adult neurogenesis, we note that *Ars2-cKO* and *cyclin D2-cKO* mice exhibit relatively similar behavioral profiles. These include increased stress response (FST, reduced immobility) and no changes in spatial memory (MWM) or anxiety-like behavior (EPM) (Jedynak et al., 2014). That these independent genetic models of suppressing adult neurogenesis converge on similar behavioral consequences supports the notion of a common functional basis for this deficit at the circuit level.

MATERIALS AND METHODS

Mouse maintenance

All mice were housed in the Memorial Sloan-Kettering Cancer Center mouse facility and treated with procedures approved by the Institutional Animal Care and Use Committee (IACUC). *Ars2-flox* transgenic mice were maintained as previously described (Andreu-Agullo et al., 2012). *hGFAP-Cre* (Stock #004600) (Zhuo et al., 2001), *Ai9* (*ROSA-loxP-STOP-loxP-tdTomato*, Stock #007909) (Madisen et al., 2010), *Nestin-CreERT2* (Stock #016261) (Battiste et al., 2007) and *Olig2-Cre* (Stock #025567) (Zawadzka et al., 2010) mice were obtained from the Jackson Laboratory. For activation of the *Nestin-CreERT2*, 4-hydroxytamoxifen (TAM) was administered via intraperitoneal injection in P30 mice, or through gavaging in adult mice over P60. Both males and females were used for phenotypic analyses. All mice were maintained with a mixed background of *C57BL6* and *129S1*.

NSC culture and differentiation

NSCs are cultured with NeuroCult Proliferation Kit (Stemcell Technologies, 05702) according to the manufacturer's manual. Briefly, adult SVZ is dissected from 6-8 week mice. Chopped tissue was enzymatically dissociated with Accutase (Stemcell Technologies, 07920), mechanically dissociated by pipetting, and cultured with NeuroCult medium containing epidermal growth factor (EGF; 20 ng/ml, Peprotech) and FGF2 (10 ng/ml, Peprotech). For the differentiation assay, cells were seeded on poly-D-lysine-coated glass coverslips and cultured in medium without EGF.

Histology, antibody and imaging

Mice were perfused intracardially with phosphate buffered saline (PBS), followed by 4% paraformaldehyde (PFA). The brain was then dissected and post fixed for 6-8 h. Brain vibratome sections at 70 µm were used for immunohistochemistry. Rabbit Ars2 antibody was a gift from Dr Xin Lu (Ludwig Institute for Cancer Research, Oxford, UK). A new goat Ars2 was made using the C terminus peptide (C-DPRAIVEYRDLDAPD) and used at 2.5 µg/ml for immunostaining and ChIP-seq and 1 µg/ml for western blotting. BEND6 antibody was made by SDIX against amino acids 101-190 (LPQAVTQFEELVGMAETLLKSGGAVSTPASTLWRATNNSSPDSFA-SLCSNSNSTSSSPSSVKAEEEQHPGEKQFTIERWQIARCNKSKPQ) and used at 2 µg/ml for immunostaining. The following commercial antibodies were used in immunostaining: rabbit anti-SOX2 (R&D Systems, AF2018, 1:200), mouse anti-NeuN (Millipore, MAB377, 1:400), goat anti-DCX (Santa Cruz Biotechnology, SC8066, 1:100), goat anti-Pax6 (BioLegend, prb-278p, 1:500), rabbit anti-cleaved Caspase-3 (Cell Signaling Technology, D175, 1:400), mouse anti-GFAP (Sigma-Aldrich, G3893, 1:1000), rabbit anti-GFAP (Dako, Z0334, 1:1000), rabbit anti-Ki67 (Thermo Fisher Scientific, RM-9106, 1:300) and rat anti-BrdU (Santa Cruz Biotechnology, SC56258, 1:400). BrdU was administered via intraperitoneal injection 30 min before sacrifice (50 mg/kg body weight). Before BrdU staining, sections were treated with HCl (1N) and washed thoroughly with PBS. EdU analysis was performed using the manufacturer's protocol (Life Technologies). Images were obtained using a Leica TCS confocal microscope and analyzed with ImageJ and Photoshop. The images of whole cerebellum, CA1 region and DG (Figs 2E,G,O, 3A,F and 4E,F) were generated by automerging confocal images using the photomerge utility in Photoshop. In some cases, merged images were manually adjusted to optimize tiling.

ChIP-seq and ChIP-qPCR

ChIP is performed largely as previously described with minor modifications (Dai et al., 2013b). In brief, 2×10^7 NSCs were harvested and cross-linked for sonication. Immunoprecipitation was performed with 4 µg rabbit or goat anti-Ars2 antibody. Normal rabbit or goat IgG was used as control. For ChIP with RNase treatment, RNase A (Roche, 11579681001) was added to the cell pellet and/or chromatin extract to 100 µg/ml. DNA libraries were made using the Illumina ChIP-seq library preparation kit and sequenced as individual lanes on the Illumina GAII. qPCR was performed with the Bio-Rad CFX96 machine using Power SYBR Green reagent (Applied Biosystems). Primers for qPCR were designed with online tools from IDT (see Table S1).

Computational analyses

Reads were mapped to the mm10 genome using Bowtie2.2.5 with default parameters (Langmead and Salzberg, 2012) and visualized by converting to wiggle coverage format using QuEST (Valouev et al., 2008). Peaks were defined with MACS2 (Feng et al., 2012). We used a conservative approach to re-apply peak calling with MACS2 (https://github.com/taoliu/MACS) (Zhang et al., 2008) and removed duplicate reads at unique-mapped locations. Note that this may underestimate the peak enrichment at highly ChIPed regions, such as *Sox2*. Peak summits were annotated to genes with the nearest TSS (within 2 million base pairs) using Refseq release 72. For *de novo* motif finding, we ran MEME-ChIP on regions with 300 bp flanking summits, searching for 6-12 nt motifs using default settings (Bailey and Elkan, 1994). We tested different classes of Ars2-bound regions across various levels of ChIP enrichment, as summarized in the text. GO analysis was carried out using GREAT v3.0 (http://great.stanford.edu/public/html/) (McLean et al., 2010).

We used published scRNA-seq data (Loo et al., 2019) to survey genes in E14.5 embryonic neocortex, focusing on the RG1 (8-E), VZ-SVZ (11-E), and SVZ (migrating) (4-E) cell populations as described (http://zylkalab.org/datamousecortex).

Behavioral procedures

All testing was performed between 8am and 5pm with 8-to 14-week-old mice. First, animals were tested for spatial memory in the MWM as described (Dumont et al., 2009). The subjects' movements in the maze were tracked and analyzed using EthoVision (Noldus Information Technology). One week after the completion of this test, innate fear/anxiety was assessed

using the EPM as previously described (Gleason et al., 2010). Numbers of arm entries and distance covered during a 10 min trial were tracked and analyzed by EthoVision. One week after the completion of the EPM test, stress-induced escape behavior was assessed using the Porsolt swim test (Porsolt et al., 1978), with mice placed into a cylinder filled with room temperature water and allowed to swim for 6 min. Immobility duration was scored from video by a blinded observer. Finally, 3 days later, animals were tested for contextual fear conditioning according to a published protocol (Pattwell et al., 2011). Freezing behavior was recorded by the FreezeFrame software (Actimetrics).

Statistical analysis

Prism (7.0c) and SPSS (20) were used to perform unpaired *t*-test, one-way ANOVA, two-way ANOVA, and repeated-measures ANOVA, as specified in the legends of each figure.

Acknowledgements

We thank Wei Shi for performing some immunostaining experiments, Chenu Jayewickrema for helping to prepare ChIP material, Jakub Westholm for preliminary ChIP analysis, and Alex Joyner for comments on this work.

Competing interests

The authors declare no competing or financial interests.

Author contributions

Conceptualization: Y.Y., E.C.L.; Methodology: Y.Y., C.A.-A., B.F.L., L.B., M.T., E.C.L.; Software: Y.Y.; Validation: Y.Y., C.A.-A., B.F.L., L.B., M.T.; Formal analysis: Y.Y., C.A.-A., M.T.; Investigation: Y.Y., C.A.-A., B.F.L., L.B.; Resources: Y.Y., C.A.-A., M.T., E.C.L.; Data curation: Y.Y., C.A.-A., M.T., E.C.L.; Writing - original draft: Y.Y.; Writing - review & editing: Y.Y., M.T., E.C.L.; Visualization: Y.Y., M.T., E.C.L.; Supervision: M.T., E.C.L.; Project administration: E.C.L.; Funding acquisition: Y.Y., E.C.L.

Funding

Y.Y. was supported by a New York State Stem Cell Science (NYSTEM) postdoctoral fellowship. Work in M.T.'s group was supported by the National Institutes of Health (RO1-NS106056). Work in E.C.L.'s group was supported by grants from NYSTEM (C028120), the National Institutes of Health (R01-NS083833 and R01-GM083300) and a Memorial Sloan-Kettering Cancer Center Core Grant (P30-CA008748). Deposited in PMC for release after 12 months.

Data availability

The Ars2, Sox2 and IgG ChIP-seq raw sequencing datasets have been deposited at the NCBI Gene Expression Omnibus under accession number GSE134106.

Supplementary information

Supplementary information available online at
http://dev.biologists.org/lookup/doi/10.1242/dev.180018.supplemental

References

Alagappan, D., Balan, M., Jiang, Y., Cohen, R. B., Kotenko, S. V. and Levison, S. W. (2013). Egr-1 is a critical regulator of EGF-receptor-mediated expansion of subventricular zone neural stem cells and progenitors during recovery from hypoxia-hypoglycemia. *ASN Neuro* **5**, 183-193. doi:10.1042/AN20120032

Amador-Arjona, A., Cimadamore, F., Huang, C.-T., Wright, R., Lewis, S., Gage, F. H. and Terskikh, A. V. (2015). SOX2 primes the epigenetic landscape in neural precursors enabling proper gene activation during hippocampal neurogenesis. *Proc. Natl. Acad. Sci. USA* **112**, E1936-E1945. doi:10.1073/pnas.1421480112

Andersen, P. R., Domanski, M., Kristiansen, M. S., Storvall, H., Ntini, E., Verheggen, C., Schein, A., Bunkenborg, J., Poser, I., Hallais, M. et al. (2013). The human cap-binding complex is functionally connected to the nuclear RNA exosome. *Nat. Struct. Mol. Biol.* **20**, 1367-1376. doi:10.1038/nsmb.2703

Andreu-Agullo, C., Maurin, T., Thompson, C. B. and Lai, E. C. (2012). Ars2 maintains neural stem-cell identity through direct transcriptional activation of Sox2. *Nature* **481**, 195-198. doi:10.1038/nature10712

Angevine, J. B.Jr. (1965). Time of neuron origin in the hippocampal region. An autoradiographic study in the mouse. *Exp. Neurol. Suppl.* Suppl. 2, 1-70.

Bailey, T. L. and Elkan, C. (1994). Fitting a mixture model by expectation maximization to discover motifs in biopolymers. *Proc. Int. Conf. Intell. Syst. Mol. Biol.* **2**, 28-36.

Battiste, J., Helms, A. W., Kim, E. J., Savage, T. K., Lagace, D. C., Mandyam, C. D., Eisch, A. J., Miyoshi, G. and Johnson, J. E. (2007). Ascl1 defines sequentially generated lineage-restricted neuronal and oligodendrocyte precursor cells in the spinal cord. *Development* **134**, 285-293. doi:10.1242/dev.02727

Benayoun, B. A., Pollina, E. A., Ucar, D., Mahmoudi, S., Karra, K., Wong, E. D., Devarajan, K., Daugherty, A. C., Kundaje, A. B., Mancini, E. et al. (2014). H3K4me3 breadth is linked to cell identity and transcriptional consistency. *Cell* **158**, 673-688. doi:10.1016/j.cell.2014.06.027

Blaiss, C. A., Yu, T.-S., Zhang, G., Chen, J., Dimchev, G., Parada, L. F., Powell, C. M. and Kernie, S. G. (2011). Temporally specified genetic ablation of neurogenesis impairs cognitive recovery after traumatic brain injury. *J. Neurosci.* **31**, 4906-4916. doi:10.1523/JNEUROSCI.5265-10.2011

Casey, B. H., Kollipara, R. K., Pozo, K. and Johnson, J. E. (2018). Intrinsic DNA binding properties demonstrated for lineage-specifying basic helix-loop-helix transcription factors. *Genome Res.* **28**, 484-496. doi:10.1101/gr.224360.117

Casper, K. B. and McCarthy, K. D. (2006). GFAP-positive progenitor cells produce neurons and oligodendrocytes throughout the CNS. *Mol. Cell. Neurosci.* **31**, 676-684. doi:10.1016/j.mcn.2005.12.006

Clarke, J. H., Tack, D., Findlay, K., Van Montagu, M. and Van Lijsebettens, M. (1999). The SERRATE locus controls the formation of the early juvenile leaves and phase length in Arabidopsis. *Plant J.* **20**, 493-501. doi:10.1046/j.1365-313x.1999.00623.x

Conboy, L., Varea, E., Castro, J. E., Sakouhi-Ouertatani, H., Calandra, T., Lashuel, H. A. and Sandi, C. (2011). Macrophage migration inhibitory factor is critically involved in basal and fluoxetine-stimulated adult hippocampal cell proliferation and in anxiety, depression, and memory-related behaviors. *Mol. Psychiatry* **16**, 533-547. doi:10.1038/mp.2010.15

Czech, B., Preall, J. B., McGinn, J. and Hannon, G. J. (2013). A transcriptome-wide RNAi screen in the Drosophila ovary reveals factors of the germline piRNA pathway. *Mol. Cell* **50**, 749-761. doi:10.1016/j.molcel.2013.04.007

Dai, Q., Andreu-Agullo, C., Insolera, R., Wong, L. C., Shi, S.-H. and Lai, E. C. (2013a). BEND6 is a nuclear antagonist of Notch signaling during self-renewal of neural stem cells. *Development* **140**, 1892-1902. doi:10.1242/dev.087502

Dai, Q., Ren, A., Westholm, J. O., Serganov, A. A., Patel, D. J. and Lai, E. C. (2013b). The BEN domain is a novel sequence-specific DNA-binding domain conserved in neural transcriptional repressors. *Genes Dev.* **27**, 602-614. doi:10.1101/gad.213314.113

Deng, W. and Gage, F. H. (2015). The effect of immature adult-born dentate granule cells on hyponeophagial behavior is related to their roles in learning and memory. *Front. Syst. Neurosci.* **9**, 34. doi:10.3389/fnsys.2015.00034

Dennis, D. J., Han, S. and Schuurmans, C. (2018). bHLH transcription factors in neural development, disease, and reprogramming. *Brain Res.* **1705**, 48-65. doi:10.1016/j.brainres.2018.03.013

Dhar, S. S. and Wong-Riley, M. T. T. (2009). Coupling of energy metabolism and synaptic transmission at the transcriptional level: role of nuclear respiratory factor 1 in regulating both cytochrome c oxidase and NMDA glutamate receptor subunit genes. *J. Neurosci.* **29**, 483-492. doi:10.1523/JNEUROSCI.3704-08.2009

Dong, Z., Han, M.-H. and Fedoroff, N. (2008). The RNA-binding proteins HYL1 and SE promote accurate in vitro processing of pri-miRNA by DCL1. *Proc. Natl. Acad. Sci. USA* **105**, 9970-9975. doi:10.1073/pnas.0803356105

Drew, M. R., Denny, C. A. and Hen, R. (2010). Arrest of adult hippocampal neurogenesis in mice impairs single- but not multiple-trial contextual fear conditioning. *Behav. Neurosci.* **124**, 446-454. doi:10.1037/a0020081

Dumont, M., Wille, E., Stack, C., Calingasan, N. Y., Beal, M. F. and Lin, M. T. (2009). Reduction of oxidative stress, amyloid deposition, and memory deficit by manganese superoxide dismutase overexpression in a transgenic mouse model of Alzheimer's disease. *FASEB J.* **23**, 2459-2466. doi:10.1096/fj.09-132928

Dupret, D., Revest, J.-M., Koehl, M., Ichas, F., De Giorgi, F., Costet, P., Abrous, D. N. and Piazza, P. V. (2008). Spatial relational memory requires hippocampal adult neurogenesis. *PLoS ONE* **3**, e1959. doi:10.1371/journal.pone.0001959

Engelen, E., Akinci, U., Bryne, J. C., Hou, J., Gontan, C., Moen, M., Szumska, D., Kockx, C., van Ijcken, W., Dekkers, D. H. W. et al. (2011). Sox2 cooperates with Chd7 to regulate genes that are mutated in human syndromes. *Nat. Genet.* **43**, 607-611. doi:10.1038/ng.825

Englund, C., Fink, A., Lau, C., Pham, D., Daza, R. A., Bulfone, A., Kowalczyk, T. and Hevner, R. F. (2005). Pax6, Tbr2, and Tbr1 are expressed sequentially by radial glia, intermediate progenitor cells, and postmitotic neurons in developing neocortex. *J. Neurosci.* **25**, 247-251. doi:10.1523/JNEUROSCI.2899-04.2005

Feng, J., Liu, T., Qin, B., Zhang, Y. and Liu, X. S. (2012). Identifying ChIP-seq enrichment using MACS. *Nat. Protoc.* **7**, 1728-1740. doi:10.1038/nprot.2012.101

Ferri, A. L. M., Cavallaro, M., Braida, D., Di Cristofano, A., Canta, A., Vezzani, A., Ottolenghi, S., Pandolfi, P. P., Sala, M., DeBiasi, S. et al. (2004). Sox2 deficiency causes neurodegeneration and impaired neurogenesis in the adult mouse brain. *Development* **131**, 3805-3819. doi:10.1242/dev.01204

Giacometti, S., Benbahouche, N. E. H., Domanski, M., Robert, M.-C., Meola, N., Lubas, M., Bukenborg, J., Andersen, J. S., Schulze, W. M., Verheggen, C. et al. (2017). Mutually exclusive CBC-containing complexes contribute to RNA fate. *Cell Rep.* **18**, 2635-2650. doi:10.1016/j.celrep.2017.02.046

Gleason, G., Liu, B., Bruening, S., Zupan, B., Auerbach, A., Mark, W., Oh, J.-E., Gal-Toth, J., Lee, F. and Toth, M. (2010). The serotonin1A receptor gene as a genetic and prenatal maternal environmental factor in anxiety. *Proc. Natl. Acad. Sci. USA* **107**, 7592-7597. doi:10.1073/pnas.0914805107

Gleeson, J. G., Lin, P. T., Flanagan, L. A. and Walsh, C. A. (1999). Doublecortin is a microtubule-associated protein and is expressed widely by migrating neurons. *Neuron* **23**, 257-271. doi:10.1016/S0896-6273(00)80778-3

Grigg, S. P., Canales, C., Hay, A. and Tsiantis, M. (2005). SERRATE coordinates shoot meristem function and leaf axial patterning in Arabidopsis. *Nature* **437**, 1022-1026. doi:10.1038/nature04052

Groves, J. O., Leslie, I., Huang, G.-J., McHugh, S. B., Taylor, A., Mott, R., Munafò, M., Bannerman, D. M. and Flint, J. (2013). Ablating adult neurogenesis in the rat has no effect on spatial processing: evidence from a novel pharmacogenetic model. *PLoS Genet.* **9**, e1003718. doi:10.1371/journal.pgen.1003718

Gruber, J. J., Zatechka, D. S., Sabin, L. R., Yong, J., Lum, J. J., Kong, M., Zong, W.-X., Zhang, Z., Lau, C.-K., Rawlings, J. et al. (2009). Ars2 links the nuclear cap-binding complex to RNA interference and cell proliferation. *Cell* **138**, 328-339. doi:10.1016/j.cell.2009.04.046

Gruber, J. J., Olejniczak, S. H., Yong, J., La Rocca, G., Dreyfuss, G. and Thompson, C. B. (2012). Ars2 promotes proper replication-dependent histone mRNA 3′ end formation. *Mol. Cell* **45**, 87-98. doi:10.1016/j.molcel.2011.12.020

Guillemot, F., Lo, L.-C., Johnson, J. E., Auerbach, A., Anderson, D. J. and Joyner, A. L. (1993). Mammalian achaete-scute homolog 1 is required for the early development of olfactory and autonomic neurons. *Cell* **75**, 463-476. doi:10.1016/0092-8674(93)90381-Y

Guo, Z., Su, Y. and Lou, H. (2018). GFAP-positive progenitor cell production is concentrated in specific encephalic regions in young adult mice. *Neurosci. Bull.* **34**, 769-778. doi:10.1007/s12264-018-0228-4

Hallais, M., Pontvianne, F., Andersen, P. R., Clerici, M., Lener, D., Benbahouche, N. E. H., Gostan, T., Vandermoere, F., Robert, M.-C., Cusack, S. et al. (2013). CBC-ARS2 stimulates 3′-end maturation of multiple RNA families and favors cap-proximal processing. *Nat. Struct. Mol. Biol.* **20**, 1358-1366. doi:10.1038/nsmb.2720

Iasillo, C., Schmid, M., Yahia, Y., Maqbool, M. A., Descostes, N., Karadoulama, E., Bertrand, E., Andrau, J.-C. and Jensen, T. H. (2017). ARS2 is a general suppressor of pervasive transcription. *Nucleic Acids Res.* **45**, 10229-10241. doi:10.1093/nar/gkx647

Iwata, Y., Takahashi, M., Fedoroff, N. V. and Hamdan, S. M. (2013). Dissecting the interactions of SERRATE with RNA and DICER-LIKE 1 in Arabidopsis microRNA precursor processing. *Nucleic Acids Res.* **41**, 9129-9140. doi:10.1093/nar/gkt667

Jaholkowski, P., Kiryk, A., Jedynak, P., Ben Abdallah, N. M., Knapska, E., Kowalczyk, A., Piechal, A., Blecharz-Klin, K., Figiel, I., Lioudyno, V. et al. (2009). New hippocampal neurons are not obligatory for memory formation; cyclin D2 knockout mice with no adult brain neurogenesis show learning. *Learn. Mem.* **16**, 439-451. doi:10.1101/lm.1459709

Jedynak, P., Kos, T., Sandi, C., Kaczmarek, L. and Filipkowski, R. K. (2014). Mice with ablated adult brain neurogenesis are not impaired in antidepressant response to chronic fluoxetine. *J. Psychiatr. Res.* **56**, 106-111. doi:10.1016/j.jpsychires.2014.05.009

Kriegstein, A. and Alvarez-Buylla, A. (2009). The glial nature of embryonic and adult neural stem cells. *Annu. Rev. Neurosci.* **32**, 149-184. doi:10.1146/annurev.neuro.051508.135600

Langmead, B. and Salzberg, S. L. (2012). Fast gapped-read alignment with Bowtie 2. *Nat. Methods* **9**, 357-359. doi:10.1038/nmeth.1923

Lessard, J., Wu, J. I., Ranish, J. A., Wan, M., Winslow, M. M., Staahl, B. T., Wu, H., Aebersold, R., Graef, I. A. and Crabtree, G. R. (2007). An essential switch in subunit composition of a chromatin remodeling complex during neural development. *Neuron* **55**, 201-215. doi:10.1016/j.neuron.2007.06.019

Li, W. and Mills, A. A. (2014). Architects of the genome: CHD dysfunction in cancer, developmental disorders and neurological syndromes. *Epigenomics* **6**, 381-395. doi:10.2217/epi.14.31

Llorens-Bobadilla, E., Zhao, S., Baser, A., Saiz-Castro, G., Zwadlo, K. and Martin-Villalba, A. (2015). Single-cell transcriptomics reveals a population of dormant neural stem cells that become activated upon brain injury. *Cell Stem Cell* **17**, 329-340. doi:10.1016/j.stem.2015.07.002

Lobbes, D., Rallapalli, G., Schmidt, D. D., Martin, C. and Clarke, J. (2006). SERRATE: a new player on the plant microRNA scene. *EMBO Rep.* **7**, 1052-1058. doi:10.1038/sj.embor.7400806

Loo, L., Simon, J. M., Xing, L., McCoy, E. S., Niehaus, J. K., Guo, J., Anton, E. S. and Zylka, M. J. (2019). Single-cell transcriptomic analysis of mouse neocortical development. *Nat. Commun.* **10**, 134. doi:10.1038/s41467-018-08079-9

Lubas, M., Christensen, M. S., Kristiansen, M. S., Domanski, M., Falkenby, L. G., Lykke-Andersen, S., Andersen, J. S., Dziembowski, A. and Jensen, T. H. (2011). Interaction profiling identifies the human nuclear exosome targeting complex. *Mol. Cell* **43**, 624-637. doi:10.1016/j.molcel.2011.06.028

Ma, Z., Castillo-González, C., Wang, Z., Sun, D., Hu, X., Shen, X., Potok, M. E. and Zhang, X. (2018). Arabidopsis serrate coordinates histone methyltransferases ATXR5/6 and RNA processing factor RDR6 to regulate transposon expression. *Dev. Cell* **45**, 769-784.e6. doi:10.1016/j.devcel.2018.05.023

Madisen, L., Zwingman, T. A., Sunkin, S. M., Oh, S. W., Zariwala, H. A., Gu, H., Ng, L. L., Palmiter, R. D., Hawrylycz, M. J., Jones, A. R. et al. (2010). A robust and high-throughput Cre reporting and characterization system for the whole mouse brain. *Nat. Neurosci.* **13**, 133-140. doi:10.1038/nn.2467

Martynoga, B., Mateo, J. L., Zhou, B., Andersen, J., Achimastou, A., Urban, N., van den Berg, D., Georgopoulou, D., Hadjur, S., Wittbrodt, J. et al. (2013). Epigenomic enhancer annotation reveals a key role for NFIX in neural stem cell quiescence. *Genes Dev.* **27**, 1769-1786. doi:10.1101/gad.216804.113

McLean, C. Y., Bristor, D., Hiller, M., Clarke, S. L., Schaar, B. T., Lowe, C. B., Wenger, A. M. and Bejerano, G. (2010). GREAT improves functional interpretation of cis-regulatory regions. *Nat. Biotechnol.* **28**, 495-501. doi:10.1038/nbt.1630

Pattwell, S. S., Bath, K. G., Casey, B. J., Ninan, I. and Lee, F. S. (2011). Selective early-acquired fear memories undergo temporary suppression during adolescence. *Proc. Natl. Acad. Sci. USA* **108**, 1182-1187. doi:10.1073/pnas.1012975108

Pevny, L. and Placzek, M. (2005). SOX genes and neural progenitor identity. *Curr. Opin. Neurobiol.* **15**, 7-13. doi:10.1016/j.conb.2005.01.016

Porsolt, R. D., Anton, G., Blavet, N. and Jalfre, M. (1978). Behavioural despair in rats: a new model sensitive to antidepressant treatments. *Eur. J. Pharmacol.* **47**, 379-391. doi:10.1016/0014-2999(78)90118-8

Prigge, M. J. and Wagner, D. R. (2001). The arabidopsis serrate gene encodes a zinc-finger protein required for normal shoot development. *Plant Cell* **13**, 1263-1279. doi:10.1105/TPC.010095

Revest, J.-M., Dupret, D., Koehl, M., Funk-Reiter, C., Grosjean, N., Piazza, P.-V. and Abrous, D. N. (2009). Adult hippocampal neurogenesis is involved in anxiety-related behaviors. *Mol. Psychiatry* **14**, 959-967. doi:10.1038/mp.2009.15

Sabath, I., Skrajna, A., Yang, X.-C., Dadlez, M., Marzluff, W. F. and Dominski, Z. (2013). 3′-end processing of histone pre-mRNAs in Drosophila: U7 snRNP is associated with FLASH and polyadenylation factors. *RNA* **19**, 1726-1744. doi:10.1261/rna.040360.113

Sabin, L. R., Zhou, R., Gruber, J. J., Lukinova, N., Bambina, S., Berman, A., Lau, C.-K., Thompson, C. B. and Cherry, S. (2009). Ars2 regulates both miRNA- and siRNA- dependent silencing and suppresses RNA virus infection in Drosophila. *Cell* **138**, 340-351. doi:10.1016/j.cell.2009.04.045

Saxe, M. D., Battaglia, F., Wang, J.-W., Malleret, G., David, D. J., Monckton, J. E., Garcia, A. D. R., Sofroniew, M. V., Kandel, E. R., Santarelli, L. et al. (2006). Ablation of hippocampal neurogenesis impairs contextual fear conditioning and synaptic plasticity in the dentate gyrus. *Proc. Natl. Acad. Sci. USA* **103**, 17501-17506. doi:10.1073/pnas.0607207103

Schulze, W. M. and Cusack, S. (2017). Structural basis for mutually exclusive co-transcriptional nuclear cap-binding complexes with either NELF-E or ARS2. *Nat. Commun.* **8**, 1302. doi:10.1038/s41467-017-01402-w

Schulze, W. M., Stein, F., Rettel, M., Nanao, M. and Cusack, S. (2018). Structural analysis of human ARS2 as a platform for co-transcriptional RNA sorting. *Nat. Commun.* **9**, 1701. doi:10.1038/s41467-018-04142-7

Sillitoe, R. V. and Joyner, A. L. (2007). Morphology, molecular codes, and circuitry produce the three-dimensional complexity of the cerebellum. *Annu. Rev. Cell Dev. Biol.* **23**, 549-577. doi:10.1146/annurev.cellbio.23.090506.123237

Snyder, J. S., Soumier, A., Brewer, M., Pickel, J. and Cameron, H. A. (2011). Adult hippocampal neurogenesis buffers stress responses and depressive behaviour. *Nature* **476**, 458-461. doi:10.1038/nature10287

Speth, C., Szabo, E. X., Martinho, C., Collani, S., Zur Oven-Krockhaus, S., Richter, S., Droste-Borel, I., Macek, B., Stierhof, Y.-D., Schmid, M. et al. (2018). Arabidopsis RNA processing factor SERRATE regulates the transcription of intronless genes. *eLife* **7**, e37078. doi:10.7554/eLife.37078

Valouev, A., Johnson, D. S., Sundquist, A., Medina, C., Anton, E., Batzoglou, S., Myers, R. M. and Sidow, A. (2008). Genome-wide analysis of transcription factor binding sites based on ChIP-Seq data. *Nat. Methods* **5**, 829-834. doi:10.1038/nmeth.1246

Wang, Z., Ma, Z., Castillo-González, C., Sun, D., Li, Y., Yu, B., Zhao, B., Li, P. and Zhang, X. (2018). SWI2/SNF2 ATPase CHR2 remodels pri-miRNAs via Serrate to impede miRNA production. *Nature* **557**, 516-521. doi:10.1038/s41586-018-0135-x

Xu, H.-T., Han, Z., Gao, P., He, S., Li, Z., Shi, W., Kodish, O., Shao, W., Brown, K. N., Huang, K. et al. (2014). Distinct lineage-dependent structural and functional organization of the hippocampus. *Cell* **157**, 1552-1564. doi:10.1016/j.cell.2014.03.067

Yang, L., Liu, Z., Lu, F., Dong, A. and Huang, H. (2006). SERRATE is a novel nuclear regulator in primary microRNA processing in Arabidopsis. *Plant J.* **47**, 841-850. doi:10.1111/j.1365-313X.2006.02835.x

Yu, Y., Chen, Y., Kim, B., Wang, H., Zhao, C., He, X., Liu, L., Liu, W., Wu, L. M. N., Mao, M. et al. (2013). Olig2 targets chromatin remodelers to enhancers to initiate oligodendrocyte differentiation. *Cell* **152**, 248-261. doi:10.1016/j.cell.2012.12.006

Zawadzka, M., Rivers, L. E., Fancy, S. P. J., Zhao, C., Tripathi, R., Jamen, F., Young, K., Goncharevich, A., Pohl, H., Rizzi, M. et al. (2010). CNS-resident glial progenitor/stem cells produce Schwann cells as well as oligodendrocytes during repair of CNS demyelination. *Cell Stem Cell* **6**, 578-590. doi:10.1016/j.stem.2010.04.002

Zhang, Y., Liu, T., Meyer, C. A., Eeckhoute, J., Johnson, D. S., Bernstein, B. E., Nussbaum, C., Myers, R. M., Brown, M., Li, W. et al. (2008). Model-based analysis of ChIP-Seq (MACS). *Genome Biol.* **9**, R137. doi:10.1186/gb-2008-9-9-r137

Zhuo, L., Theis, M., Alvarez-Maya, I., Brenner, M., Willecke, K. and Messing, A. (2001). hGFAP-cre transgenic mice for manipulation of glial and neuronal function in vivo. *Genesis* **31**, 85-94. doi:10.1002/gene.10008

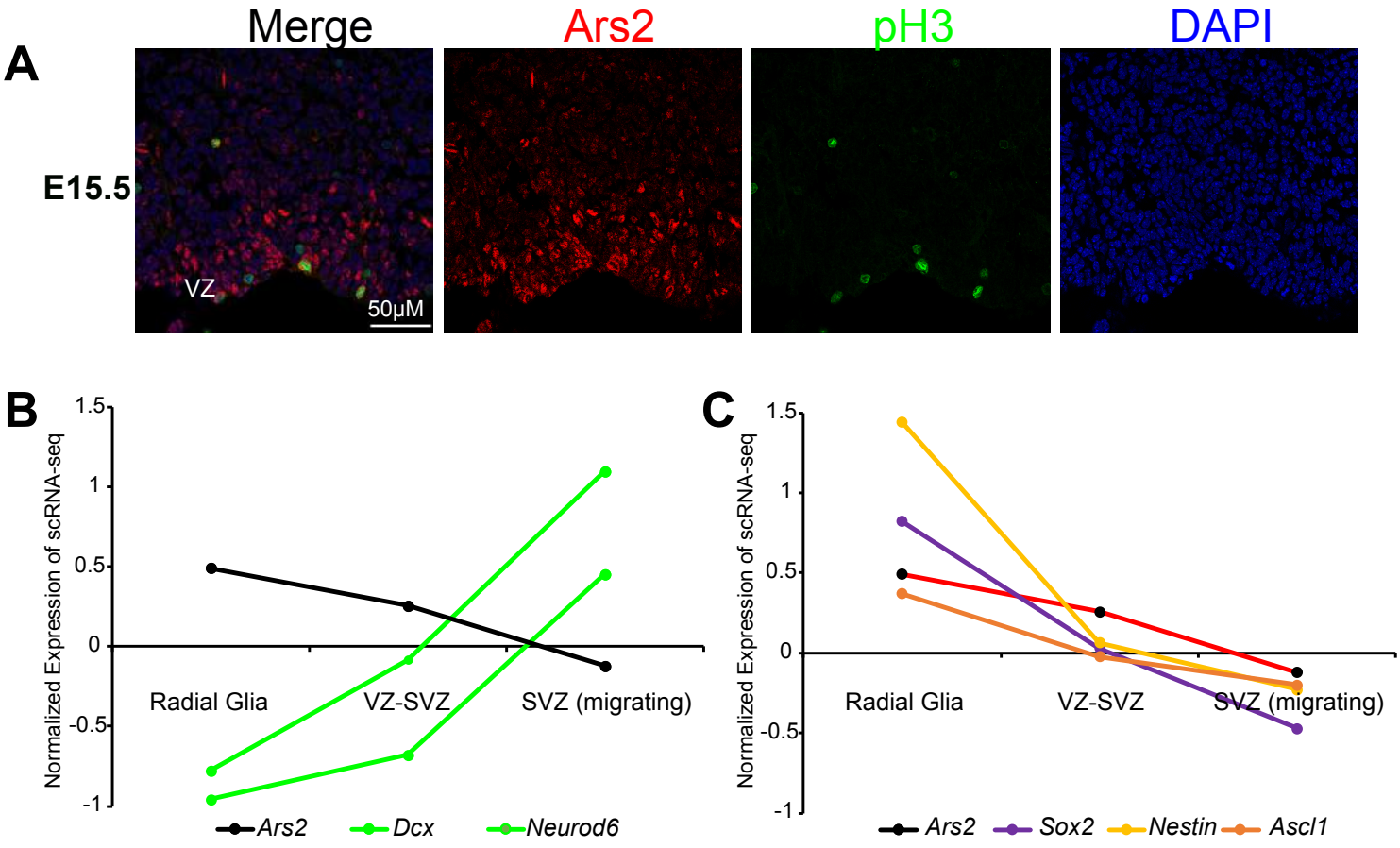

Figure S1. Additional characterization of Ars2 expression.

(A) A minority of ventricular zone (VZ) nuclei coexpress phosphohistone H3 (pH3), but most VZ nuclei are Ars2+/pH3-. Overall, Ars2 protein decreases in the subventricular zone (SVZ). (B-C) Single cell RNA-seq data (from Loo et al, 2019) recapitulates the immunostaining pattern of Ars2 protein and other celltype markers. (B) Ars2 transcripts are higher in neural stem cells (radial glia), and progressively lower in the VZ-SVZ population to migrating SVZ cells. This pattern is opposite to the progressively increasing pattern of neuroblast marker Dcx and neuronal marker Neurod6. (C) Pattern of Ars2 in these cell populations is similar to known NSC markers.

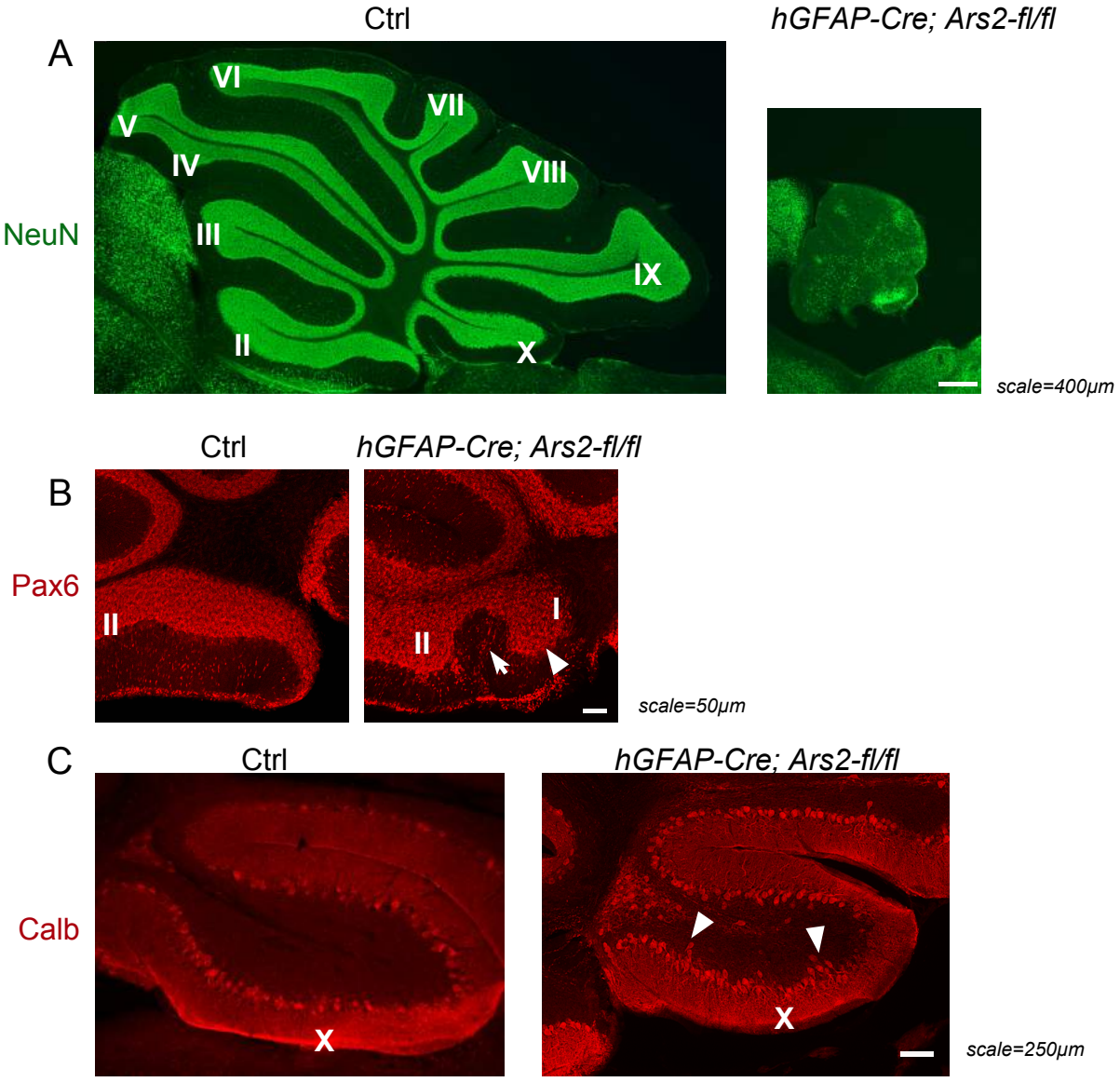

Figure S2. Phenotypic analysis of Ars2 knockout cerebellum.

(A) Sagittal sections of P15 cerebellar vermis from hGFAP-Cre; Ars2fl/fl mouse with strong phenotype and control littermate were stained with NeuN. Scale bar = 400μm.
(B) Sagittal sections of P15 cerebellum from hGFAP-Cre; Ars2fl/fl mouse with weak phenotype and control littermate were stained with Pax6. Arrow indicates the appearance of central fissure. Arrowhead indicates lobule I. Scale bar = 50μm
(D) Sagittal sections of P25 cerebellum from hGFAP-Cre; Ars2fl/fl mouse with weak phenotype and control littermate were stained with Calbindin (Calb) antibody. Arrowheads indicate the multilayered Purkinje cells. Scale bar = 250μm.

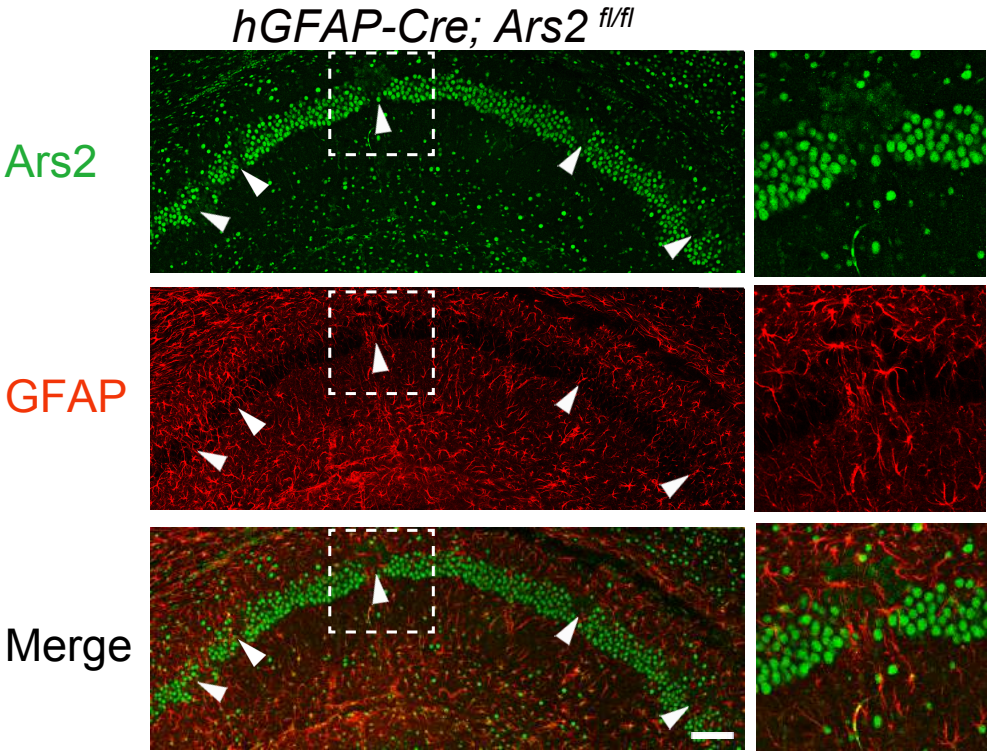

Figure S3. Ars2 deletion leads to astrogliogenesis.

P12 hGFAP-Cre; Ars2fl/fl hippocampal CA1 area stained with Ars2 (green) and astrocyte marker GFAP (red). Arrowheads and zoomed area indicate mosaic Ars2 knockout regions with ectopic GFAP expressing cells. Scale bar=100μm.

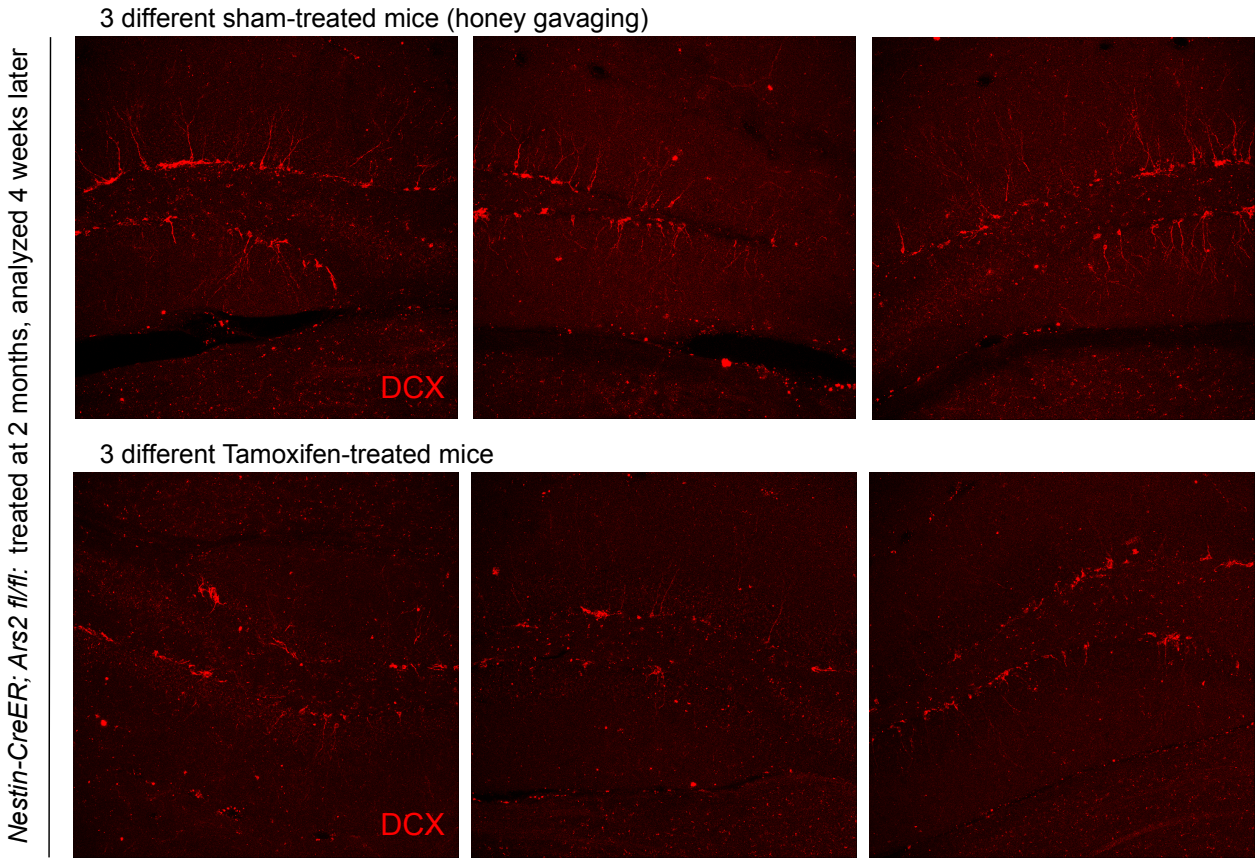

Figure S4. Adult hippocampal neurogenesis is compromised by conditional ablation of Ars2 in neural stem cells.

Representative independent Nestin-CreERT2; Ars2-fl/fl mice were sham treated (honey gavaging) or tamoxifen treated at two months of age, and dissected and stained for Doublecortin (Dcx) stainings four weeks later. The tamoxifen treated animals exhibited substantial decreases in numbers and branching of total Dcx+ neuroblasts in the dentate gyrus. Mice from this protocol were used for behavioral analysis.

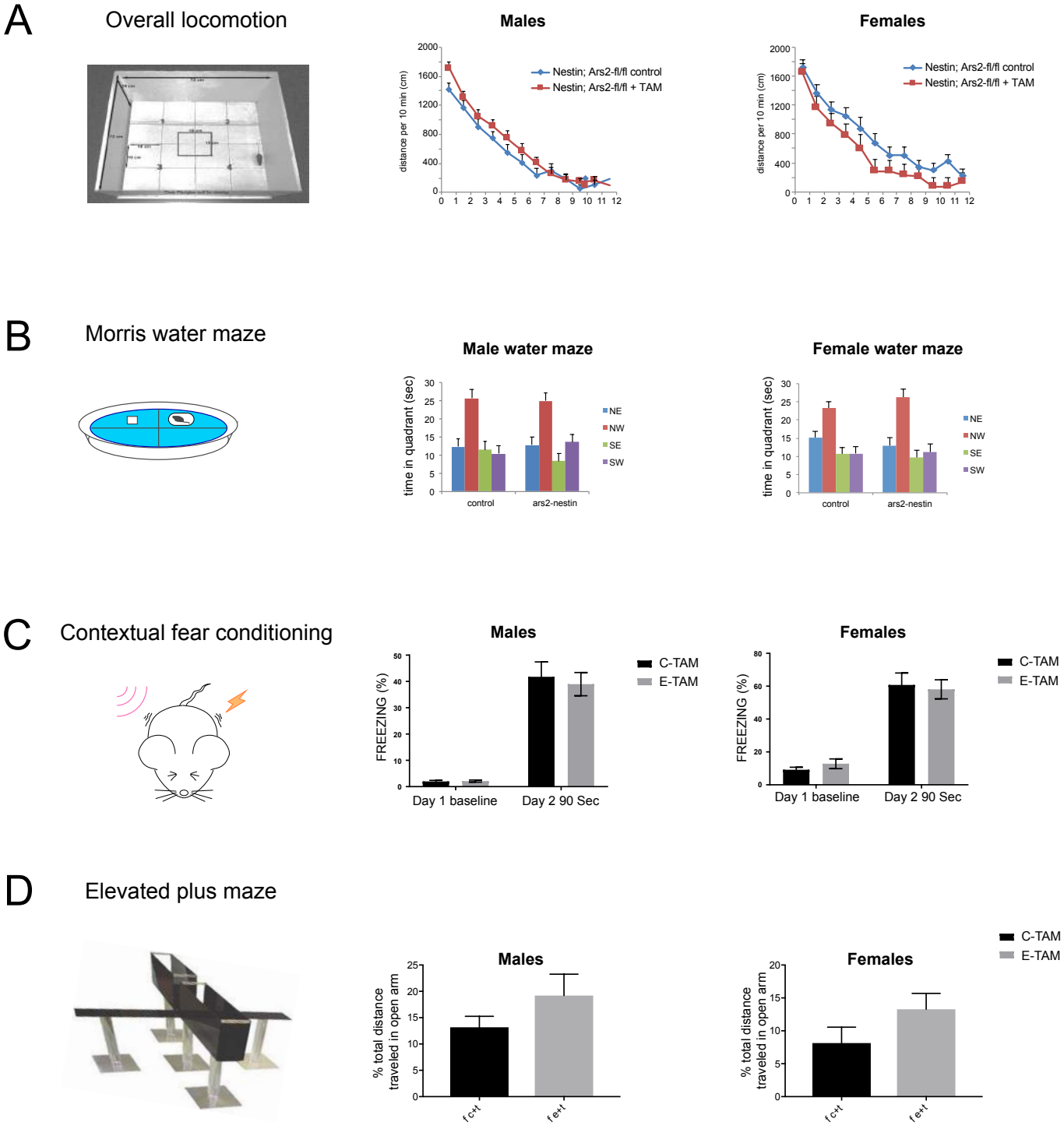

Figure S5. Testing the behavioral consequences of adult-specific ablation of Ars2 in neural stem cells.

(A) Conditional KO of Ars2 does not alter overall locomotor activity in open field. C-W=control wild type, E-TAM=Cre+ Ars2-/- injected with TAM.
(B) The spatial memory of Ars2 cKO mice in the MWM is intact. Groups same as in A.
(C) cKO mice have a control level of fear at baseline (day 1) and one day after contextual fear conditioning (day 2). Time of freezing in % of total time. C-TAM=control Ars2-/- injected with TAM, E-TAM=Cre+ Ars2-/- injected with TAM. Two way group x day ANOVA. Males, group effect $F(1,50)=0.1145$, $P=0.7365$, $N=31, 21$. Females, group effect $F(1,39)=0.008251$, $P=0.9281$, $N=18, 23$.
(D) Ars2 cKO and control mice have similar levels of innate anxiety in the EPM. Distance traveled in the open arm vs. total distance in %. Groups same as in C. Males, unpaired t-test. $t=1.441$ $df=50$, $p= 0.1557$, $N=31, 21$. Females, $t=1.483$ $df=36$, $p=0.1467$, $N=17, 21$.

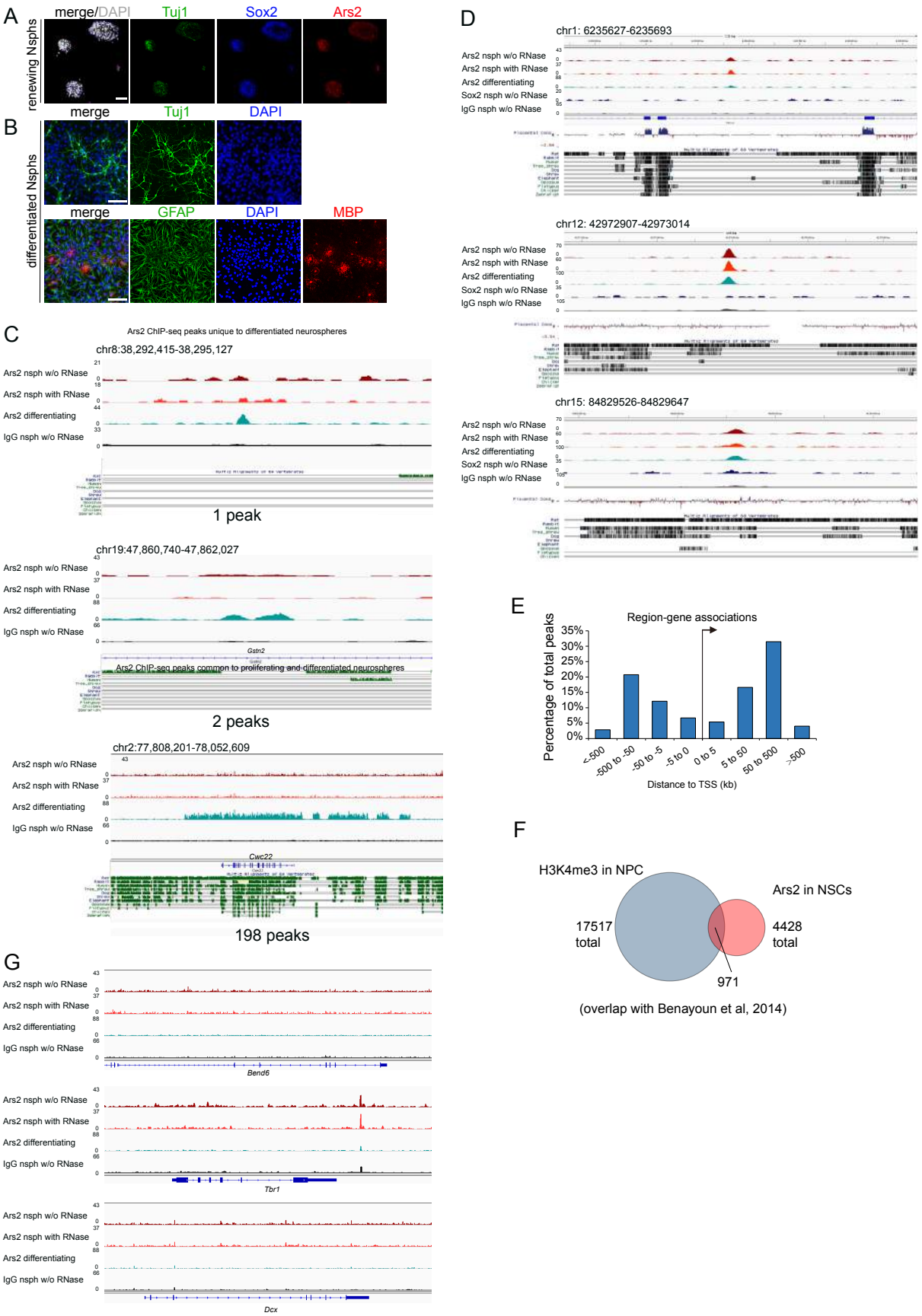

Figure S6. Ars2 associates with cis-elements in neurospheres, a model of neural stem cells.
(A-B) Confocal images of primary cultured proliferating and differentiating neurospheres. Scale bar=100μm.
(C) Enrichment profiles at representative loci with Ars2 binding only in differentiating neurospheres. The non-genic regions generally show low conservation during evolution. The example of *Cwc22* locus exhibits intensive Ars2 binding in differentiated neurospheres.
(D) Enrichment profiles at representative loci with Ars2 binding in both proliferating and differentiated neurospheres. As a class, these regions also show low evolutionary conservation.

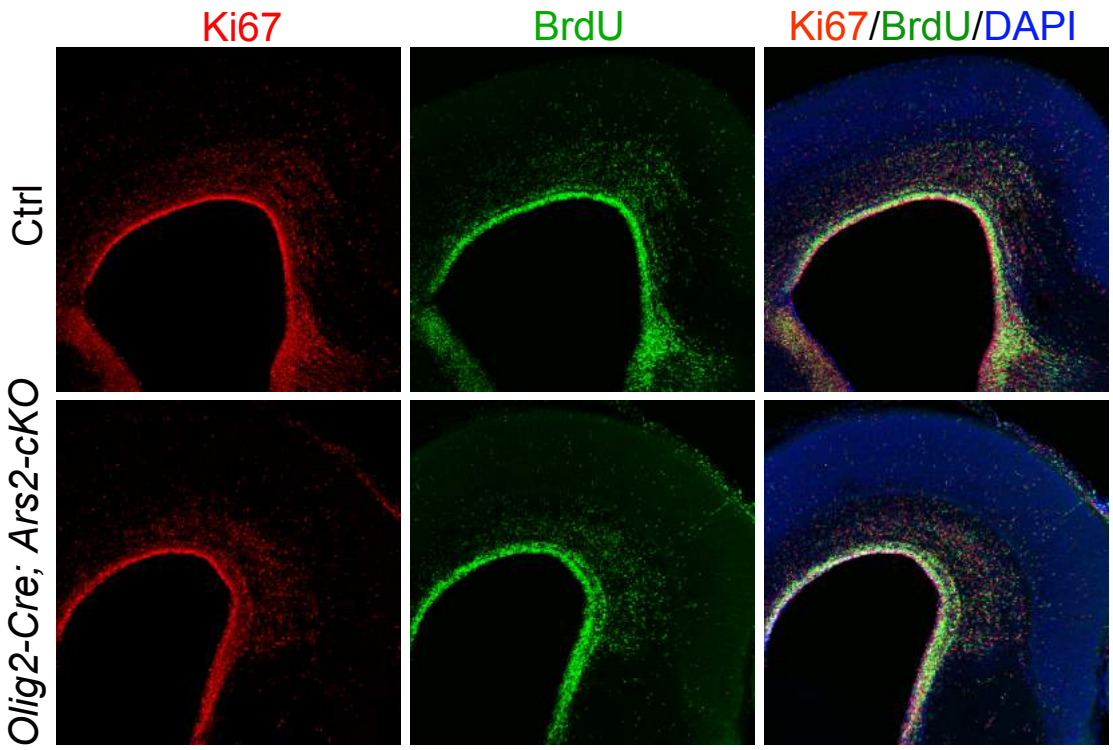

Figure S7. Cell proliferation in dorsal VZ does not change in Olig2-Cre; Ars2-cKO mice.

Confocal images of Olig2-Cre; Ars2-fl/+ control (Ctrl) and Olig2-Cre; Ars2-fl/fl mouse dorsal forebrain stained with the antibodies to Ki67 (red), BrdU (green) and with DAPI (blue) at E15.5. Consistent with the lack of expression of Olig2-Cre in dorsal VZ at this stage, no proliferation change was observed in this region, in contrast to the ventral VZ (see Figure 6F).

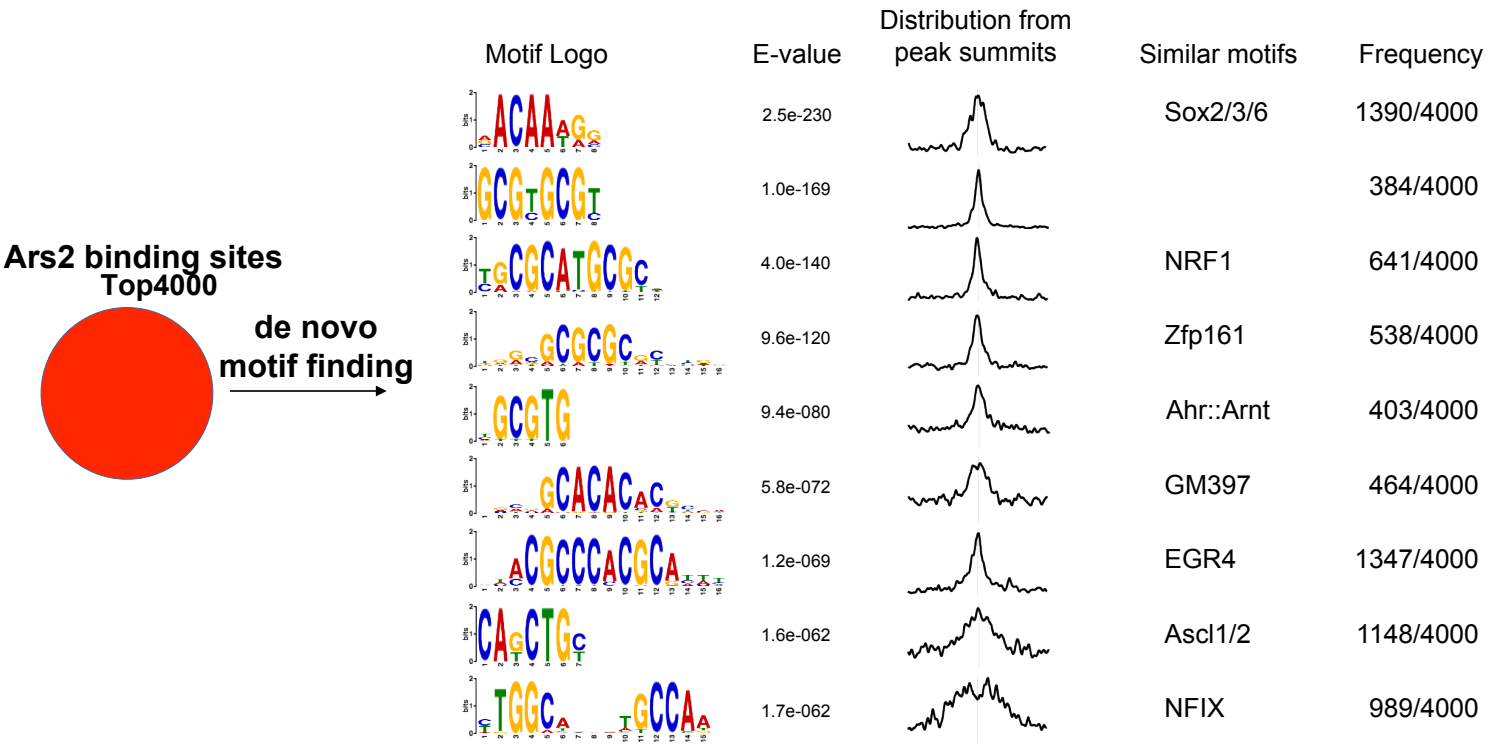

Figure S8. De novo motif discovery using of Ars2 ChIP-seq sites in proliferating neurospheres.

Motifs were derived using the top 4000 most enriched Ars2 sites that were common to ChIP-seq datasets made without and with RNase treatment from self-renewing neurosphere cultures.

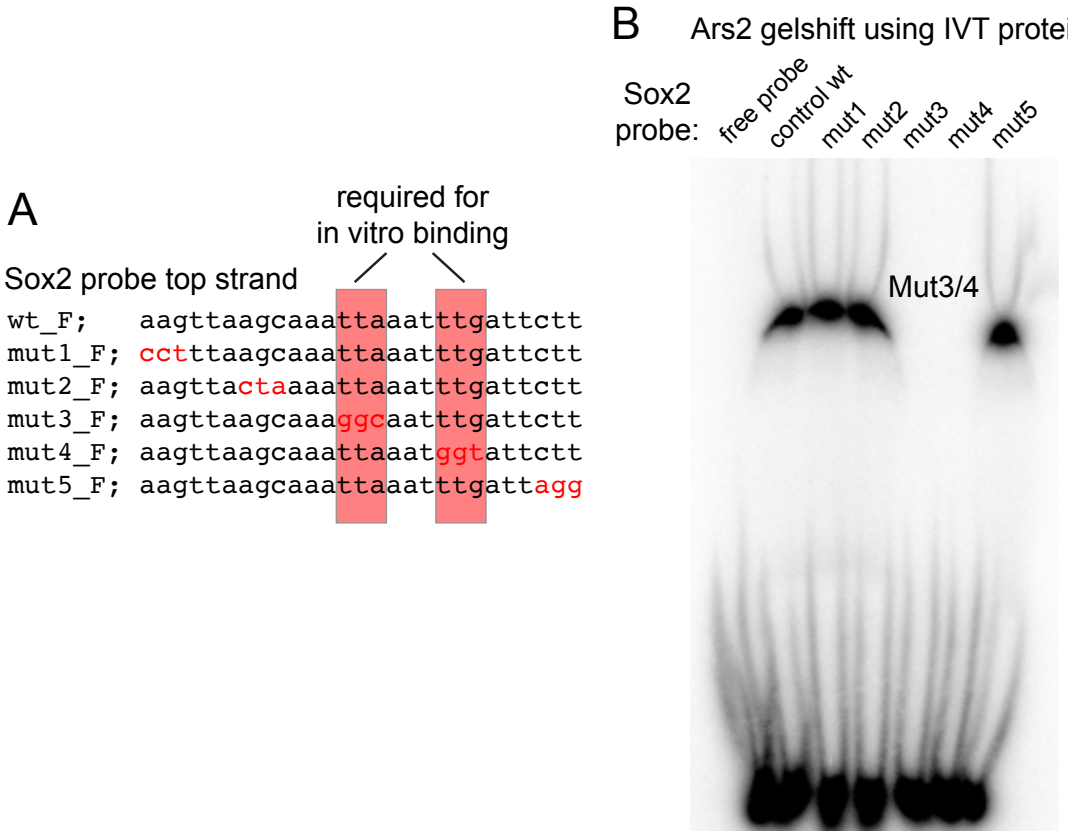

Figure S9. Scanning mutant gel-shift analysis of the Ars2 binding site in the Sox2 enhancer.
(A) Wildtype and mutant Sox2 sequences tested for binding in gel shift tests using in vitro-translated (IVT) Ars2 protein. The top strand sequences of the Sox2 probes are shown, with mutations shown in red.
(B) Gel shift tests show that Sox2 mutant probes #3 and #4 failed to interact with IVT Ars2 protein.
(C) UCSC genome browser of the Sox2 regulatory region; the 27 bp region directly tested in gel-shift analysis is marked with a black bar, with locations of mutant probes #3 and #4 indicated in pink.

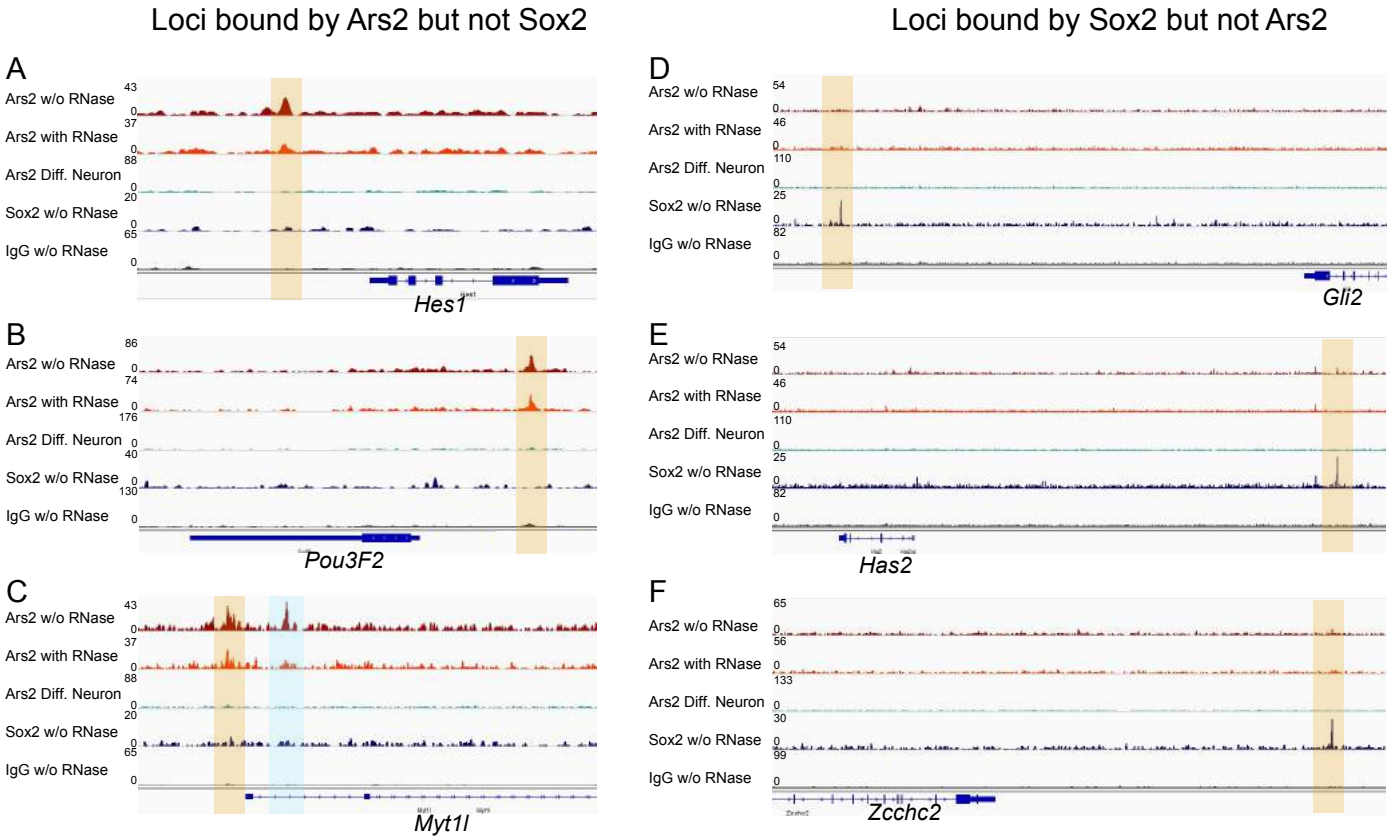

Figure S10. Examples of Ars2 and Sox2 ChIP-seq data on non-overlapping target loci.

(A-C) Example loci targeted by Ars2 but not Sox2 in proliferating neurospheres.
(D-F) Example loci targeted by Sox2 but not Ars2 in proliferating neurospheres.

Table S1. qPCR primers

Click here to Download Table S1